MATERIAL AND STRUCTURAL BEHAVIOR OF MASONRY:

SIMULATION WITH A COMMERCIAL CODE

Comportamento della muratura dal punto di vista
materiale e strutturale:
simulazioni con un codice di calcolo commerciale

Supervisor:
Prof. **Ferdinando Auricchio**

Co-supervisor: Author:
Dr. Ing. **Andrea Penna**   **Giulia Grecchi**

Abstract

Masonry is a typical composite structural material, that consists of units and mortar. Masonry structures are very common in the World, even in seismic areas where they undergo important damages and collapse. In fact, masonry is well suited to withstand high compressive loads, but it cannot bear bending and shear developed during earthquakes. Nevertheless, this material was used not only for "simple" structures (such as small houses) but also for huge monuments (like churches and cathedrals). It is important to point out that, up to some time ago, no laws were written to prescribe how to build with masonry; this led to a very different way of building from place to place, from structure to structure.

During the last decades, research on masonry behavior during earthquake has been considerably improved and a material adequate also in seismic areas was developed, using also high strength mortars and good quality units.

Nowadays, the need for structure modeling and analysis tools is largely diffused: very sophisticated finite element models or extremely simplified methods are commonly used for the seismic analysis of masonry structures, but finding a unique model is not realistic because masonry structures differ in materials, texture and structural details.

The subject of this thesis deals with the modeling of masonry, starting from a comparison with simple static tests performed during an experimental campaign carried out by University of Pavia and EUCENTRE. The principal aim is to reproduce the same results of experimental tests, through numerical modeling. A "homogenization" of the material was chosen, trying to take advantage of constitutive laws already implemented in the software and using equivalent materials to model masonry.

The work done analyzed a variety of materials with the aim to find the one

that best approximates the available experimental data for comparison. Numerical tests start with the calibration of the parameters on a simple compression test under uni-axial condition, and then continued with their validation with other characterization tests.

The decision to try an equivalent material was due to the fact that the final object was to eventually simulate the seismic tests on three prototypes of real 3D houses. This choice permits not to have an excessive computational burden to be faced.

The following script is divided into four parts:

- Chapter I describes in details the research program carried out by University of Pavia and EUCENTRE for characterizing the seismic behavior of undressed double-leaf stone masonry.

- Chapter II is a review of all the modeling techniques, available in literature and implemented for masonry structures.

- Chapter III describes the computational code Abaqus.

- Chapter IV focuses on the material chosen for simulations and presents the results find out during simulations.

- Chapter V briefly describes a User Material found in literature.

- Chapter VI discusses possible future developments on masonry modeling.

Sommario

La muratura è un tipico materiale strutturale composto da blocchi e malta. Le strutture in muratura sono molto diffuse nel mondo, anche nelle zone sismiche dove subiscono importanti danni e spesso collassano. Infatti la muratura sopporta bene elevati carichi di compressione, ma non può sopportare momenti e tagli che si sviluppano durante gli eventi sismici. Nonostante tutto però, questo materiale è stato usato non solo per costruire semplici strutture (come possono essere piccole case), ma anche grandi monumenti (come chiese e cattedrali). E' importante sottolineare che fino a poco tempo fa, nessuna legge regolamentava come costruire con la muratura; tutto ciò ha portato a diversi metodi di costruzione che cambiano non solo da posto a posto, ma anche da struttura a struttura.

Negli ultimi decenni, la ricerca nel campo del comportamento della muratura è cresciuta notevolmente: grazie anche all'uso di malte ad alta resistenza e blocchi di buona qualità è stato possibile ottenere un materiale adeguato anche in zona sismica.

Attualmente, si è diffusa la necessità di modellare le strutture in muratura con strumenti di analisi adatti: sono in uso per l'analisi simica, sia modelli molto sofisticati agli elementi finiti, sia metodi notevolmente semplificati; un modello unico non è pensabile in quanto le strutture in muratura differiscono per materiali, struttura e dettagli costruttivi.

L'oggetto di questa tesi è la modellazione della muratura partendo dal confronto con prove statiche eseguite durante una campagna sperimentale eseguita presso l'Università di Pavia ed EUCENTRE. L'obbiettivo principale è quello di ottenere gli stessi risultati dei test sperimentali attraverso una simulazione numerica. Si è scelto di operare una "omogenizzazione del materiale, cercando di

sfruttare le leggi costitutive già implementate nel software.

Il lavoro svolto ha compreso l'analisi di diversi materiali per trovare quello che approssima meglio i dati sperimentali disponibili per il confronto. I test sperimentali cominciano con la calibrazione dei parametri attraverso un test di compressione semplice in condizioni monoassiali e proseguono con la validazione attraverso gli altri test di caratterizzazione.

La decisione di utilizzare un materiale equivalente è stata presa pensando all'obbiettivo finale del lavoro di simulare le prove sismiche condotte su tre prototipi in 3D. Questa scelta, infatti, permette di non avere un onere computazionale eccessivo.

Il seguente elaborato è diviso in quattro parti:

- Il Capitolo I descrive in dettaglio il programma di ricerca eseguito presso l'Università di Pavia ed EUCENTRE per caratterizzare il comportamento sismico della muratura in pietra a doppio paramento.

- Il Capitolo II passa in rassegna tutte le tecniche di modellazione disponibili in letteratura e implementate per le strutture in muratura.

- Il Capitolo III descrive il codice di calcolo utilizzato (Abaqus).

- Il Capitolo IV ha come argomento i materiali presi in considerazione nelle analisi e i risultati prodotti con le simulazioni di calcolo.

- Il Capitolo V descrive brevemente lo User Material trovato in letteratura.

- Il Capitolo VI conclude il lavoro con una panoramica dei possibili sviluppi futuri nella modellazione della muratura.

Acknowledgements

I am very grateful to Prof. Auricchio for his continuous helpfulness, his wise advice and his sincere incitement during all this thesis.

I would like to thank Dr. Eng. Andrea Penna and Dr. Eng. Maria Rota for their valuable help and all the constructive support they gave me during these months.

I gratefully acknowledge the priceless help of Prof. Dhanasekar from QUT (Queensland University of Technology): I was pleasantly surprised by his kindness in sending me his subroutine.

I really want to thank the always helpful suggestions of the whole CompMec lab's members: their support was essential, but their patience was sorely tested!

Contents

List of Figures

List of Tables

Chapter 1

Experimental Program

In Italy, undressed double-leaf stone masonry is a common building technique in existing buildings, but experimental tests are not so many and computational modeling of masonry is a research field that need more efforts.

University of Pavia and EUCENTRE carried out an experimental program on the seismic behavior of undressed double-leaf stone masonry within the framework of ReLUIS[1] and EUCENTRE Research Programs [2]. The whole research program is fully described in [18, 19]. Here a brief summary of what was done is presented.

The experimental campaign was organized in three different steps:

1. First of all the important choice of materials (mortar and units) and construction techniques (double-leaf), with the purpose of reproducing the typical conditions of old buildings (described in section 1.1);

2. Then the execution of tests (vertical compression, diagonal compression and in-plane cyclic shear test) to characterize the mechanical properties of the chosen masonry (explained in section 1.2);

3. The execution of shake-table tests on three full scale prototype buildings.

---

[1]Linea 1- Programma di Ricerca ReLUIS: "Valutazione e riduzione della vulnerabilità di edifici in muratura" (Italian)
[2]Research Programm n. 2 - Executive Project for 2005-2008

1.1   The double-leaf stone wall

The masonry type, used in this research program, reproduces old masonry typical in Italy (figure 1.1). Walls are built with two leaves of stones connected with few transverse elements (through stones). This connection, together with the mechanical properties of the materials used and the construction quality, are responsible of the behavior of the whole panel. The number of through stones derives from traditional rules of thumbs, thus sometimes this transverse stones are missing and the interaction between the two leaves depends only on friction between blocks. This fact can lead to very dangerous failure modes with loss of wall integrity and structure collapse.

Figure 1.1: Double-leaf masonry (wall cross section)

Another important and uncertain factor in this construction technique is the amount of mortar used between the stones in the wall. Infact, when units are rough dressed stones or of extremely variable dimensions, a large amount of mortar is needed[3], affecting the strength properties of the panel. The mortar must be well confined by units, otherwise local instability may occur with localized compression cracks that develop in vertical and horizontal joints.

Double-leaf stone walls are extremely heterogeneous, that means it is very difficult to predict mechanical properties of masonry looking only at its compo-

---

[3]Sometimes when large amount of mortar is needed, it is common use to add chips of stones to reduce the mortar volume.

Figure 1.2: Structure collapse in Pescomaggiore, AQ (6th April 2009)

nents' characteristics. In order to predict the structural behavior of such masonry, experimental information derived from tests is essential.

1.1.1   The stones

To reproduce the ancient technique of double-leaf stone walls, the choice of materials and building techniques was made to create a representation of what can be found in old existing buildings in Italy.

Figure 1.3: Credaro Stone

The natural stone selected was the Credaro stone (figure1.3), which is a

sedimentary rock made of calcareous sandstone. This stone comes from near Bergamo and was widely used as a building material in the past for its good mechanical properties (which are shown in table 1.1).

Table 1.1: Credaro stone mechanical properties

Density	$2579 \, \mathrm{Kg/m^3}$
Compressive strength	$165 - 172 \, \mathrm{MPa}$
Flexural strength	$19 \, \mathrm{MPa}$

1.1.2   The mortar

Also mortar had to be produced in a special way, in order to obtain something similar to the mortar typical of historical buildings. The desired mortar should not exceed $2 \, \mathrm{MPa}$ of compression strength, while current mortars have higher value for this characteristic.

The company Tassullo produced a pre-mixed natural hydraulic lime mortar which was the basis of the mortar used. The initial product (T30V), used to restore historical buildings, belongs to the CSIII class, according to the European Standard EN 1015-11.

The initial resistance between $3.5 \, \mathrm{MPa}$ and $7.5 \, \mathrm{MPa}$ was appositely reduced for these experimental tests, by adding a certain quantity of sand to the mix. Several trials had to be done, but finally the proportions were as follows:

1. 22%: ratio of sand and mortar volume;

2. 18%: ratio of sand and mortar weight.

Because of the curing time of the mortar, specimens had to be tested when the mechanical properties of the mortar have became stable.

With standardized laboratory tests, it is possible to obtain the main mechanical characteristics of the mortar: the tensile resistance is calculated from flexural failure, while compressive strength is evaluated with compression tests.

According to EN1015-11, specimens dimension are $160 \times 40 \times 40 \, \mathrm{mm}$, and tests were carried out at different curing times (from 7 to over 90 days) in order

to collect information on the evolution of mechanical properties over time. The most important compression tests were the ones performed after 28 days and 60 days. The resistance reached after 28 days is very close to the maximum value and the curing process is considered completed after 60 days.

In figure 1.4 the mean values of compressive strength (plus or minus standard deviation) for different curing periods is shown. Mean values of compressive strength obtained after 28 and 60 days ($1.71\,\mathrm{MPa}$ and $1.78\,\mathrm{MPa}$, respectively), do not change much, though a large number of samples were tested. Some specimens were tested after 90 and 200 days, but the scarcity of data does not allow to state that resistance is subjected to changes with passing of time.

Mechanical properties of this mortar can be considered constant after 30 days of curing. The small number of specimens tested after 90 days or 200 days does not allow to conclude the resistance significantly varies further with time.
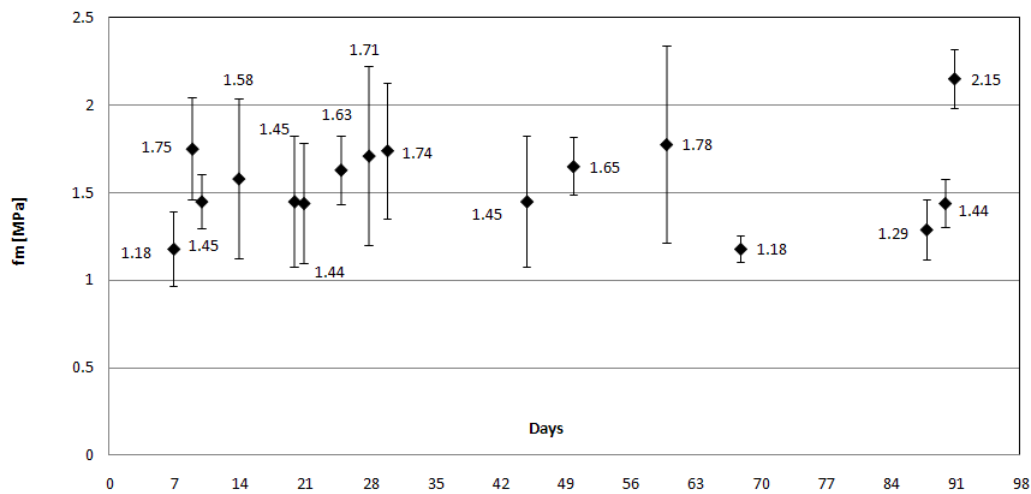
Figure 1.4: Compressive strength (plus or minus standard deviation) for different curing periods

Table 1.2: Results: compression on mortar specimens

Proportion	Curing time	Compression strength	Standard deviation
Proportion 1.	28 days	$1.71\,\mathrm{MPa}$	$0.51\,\mathrm{MPa}$
Proportion 2.	60 days	$1.78\,\mathrm{MPa}$	$0.56\,\mathrm{MPa}$

1.1.3   Specimens

In order to obtain a pseudo-prismatic shape (between $200 - 350\,\mathrm{mm}$ in height and $100 - 150\,\mathrm{mm}$ in width), the stones were worked with hammer and then placed on mortar layers trying to create horizontal courses. No through stones were placed in the wall except for the edges. The space between the two wythes was fulfilled with mortars and stone fragments; this space changed from point to point, since the element size was quite variable. Even the mortar layers changed in thickness, going from $20\,\mathrm{mm}$ to $30\,\mathrm{mm}$ at some points. The wall was $320\,\mathrm{mm}$ deep, and this is the same thickness adopted for the prototypes to be tested on the shake table.

The experimental program included tests with specific standards described for new masonry typologies and extended, in this work, for the historical masonry analyzed. To decide the specimens' size, an average size of the units was considered and the results are:

1. vertical compression tests were carried on 6 specimens with nominal dimensions of $1200 \times 800 \times 320\,\mathrm{mm}$

2. diagonal compression tests were carried on 6 specimens with nominal dimensions of $1000 \times 1000 \times 320\,\mathrm{mm}$

Specimens were obtained by cutting a unique long wall, in order to avoid edge effects. In this way, specimens can be assumed to be representative of a theoretically homogeneous masonry layout, avoiding edge effect of through stones (figure 1.5).

The wall was then confined with vertical steel wires (to limit the damage during the cut, figure 1.5) and cut with an electric circular saw after a curing time of about two and a half months. Specimens for vertical compression had two concrete tie beams built before the cut, to facilitate transportation and to distribute the load transmitted to the wall during testing. This procedure was not used for the wall designed for diagonal compression, since it would have affected the test.

Figure 1.5: Wall edge before cut (left) and after cut (right)

1.2 Tests

1.2.1 Vertical compression tests

In vertical compression tests, the specimens are subjected to monotonic or cyclic compression force. This resultant force must be kept in the centre of the wall section trying to generate a uniform vertical stress in the specimen. As the load increases, the deformation is determined directly on the wall. With this test, two important characteristics of the material can be evaluated in the pseudo-elastic behavior range: the masonry stiffness (Young's modulus E) and Poisson's ratio ν. Moreover, if tests are done up to failure, the ultimate strength and the deformation capacity in compression can be studied.

The test apparatus is made up of a force-controlled press device (figure 1.6), while displacements were measured with 8 *Gefran PZ-12-A-50* displacement transducers, placed on the specimens as shown in figure 1.7. Transducers are placed according to EN1052-1 standards, which prescribes that :

1. the distance between two transducers placed on the same wall side should be approximately equal to half the width of the wall side itself;

Figure 1.6: Vertical compression test setup

2. the initial length of the vertical transducers should be nearly $h/3$, where h is the total height of the specimen.

Figure 1.7 shows that, four transducter were placed to measure vertical deformations (number 1, 2, 4 and 5; length around $600\,\mathrm{mm}$), two for deformation in the horizontal plane (number 3 and 6; length around $400\,\mathrm{mm}$) and two for transverse horizontal displacements (number 7 and 8; length $20\,\mathrm{mm}$).

Let l_{0i} be the initial length of the ith potentiometer, the deformation corresponding to the ith potentiometer ε_i, can be determined as:

$$\varepsilon_i = \frac{(\Delta l)_i}{l_{0i}} \tag{1.1}$$

and the mean deformation is:

$$\varepsilon_{vert} = \frac{\sum_{k=1}^{4} \varepsilon_{v,k}}{4} \tag{1.2}$$

where $\varepsilon_{v,k}$ represents the single vertical deformation of each potentiometer.
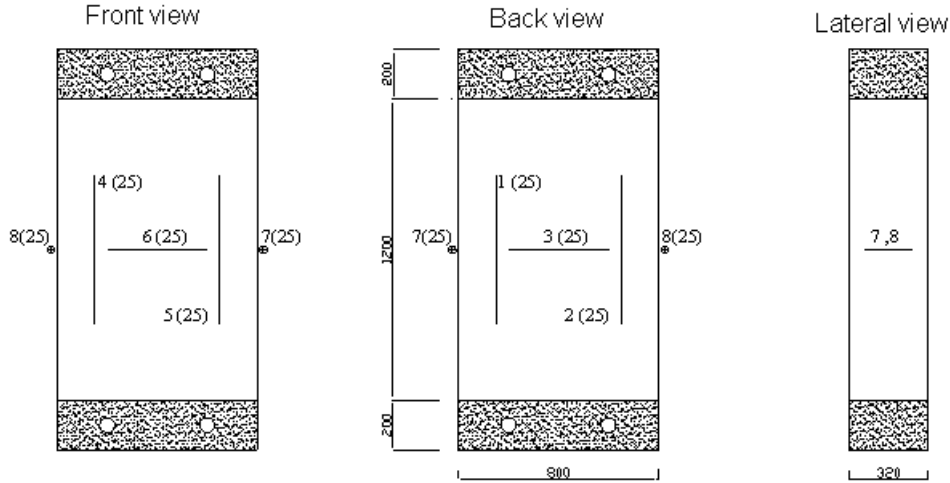
Figure 1.7: Transducers on specimens (measures in mm)

As for vertical deformation, horizontal (eq.1.3) and transverse (eq. 1.4) deformation are:

$$\varepsilon_{hor} = \frac{\sum_{k=1}^{2} \varepsilon_{h,k}}{2} \tag{1.3}$$

$$\varepsilon_{transv} = \frac{\sum_{k=1}^{2} \varepsilon_{t,k}}{2} \tag{1.4}$$

The specimens were subjected to cyclic loading of increasing intensity (table 1.3). The maximum load of each cycle was kept constant for about 60 seconds before unloading; it is assumed that this is the time needed to stabilize the state of stress in the specimens.

Young's modulus in compression is computed as:

$$E = \frac{\sigma_{v,el}}{\varepsilon\left(\sigma_{v,el}\right)} \tag{1.5}$$

where $\sigma_{v,el}$ is one third of the compressive strength $f_m = \sigma_{v,max}$ measured in the specimen.

Table 1.3: Loading cycle and nominal average compression for compression tests

Compression	Load
0.2 MPa	51 kN
0.4 MPa	102 kN
0.6 MPa	154 kN
1.0 MPa	256 kN
1.4 MPa	358 kN
1.8 MPa	461 kN
2.2 MPa	563 kN
2.6 MPa	666 kN
3.0 MPa	768 kN
3.4 MPa	870 kN
3.8 MPa	973 kN

The equivalent Poisson's ratio is defined for the horizontal and the transverse direction separately, because of the strong anisotropy of the material:

$$\nu_{hor} = \frac{\varepsilon_{hor}\left(\sigma_{v,el}\right)}{\varepsilon_{vert}\left(\sigma_{v,el}\right)} \tag{1.6}$$

$$\nu_{transv} = \frac{\varepsilon_{transv}\left(\sigma_{v,el}\right)}{\varepsilon_{vert}\left(\sigma_{v,el}\right)} \tag{1.7}$$

These parameters are calculated with the hypothesis of monotonic compression, thus deformation depends only on the level of vertical compression and boundary conditions do not have any influence on the state of stress of the specimen. This hypothesis is supposed to be true near the middle section of the panel, where the instrumentation was fixed. Nevertheless, in the transverse direction it was quite hard to place the transducers exactly in the middle, and this fact reduces the confidence of results.

Six specimens were tested; figure 1.8 represents typical results available from this kind of tests: the upper side shows the applied force over time while in the lower side there is the $\sigma - \varepsilon$ trend of the sixth test (this test is the one taken into account during simulations).

Table 1.4 shows a summary of the results of the vertical compression tests.
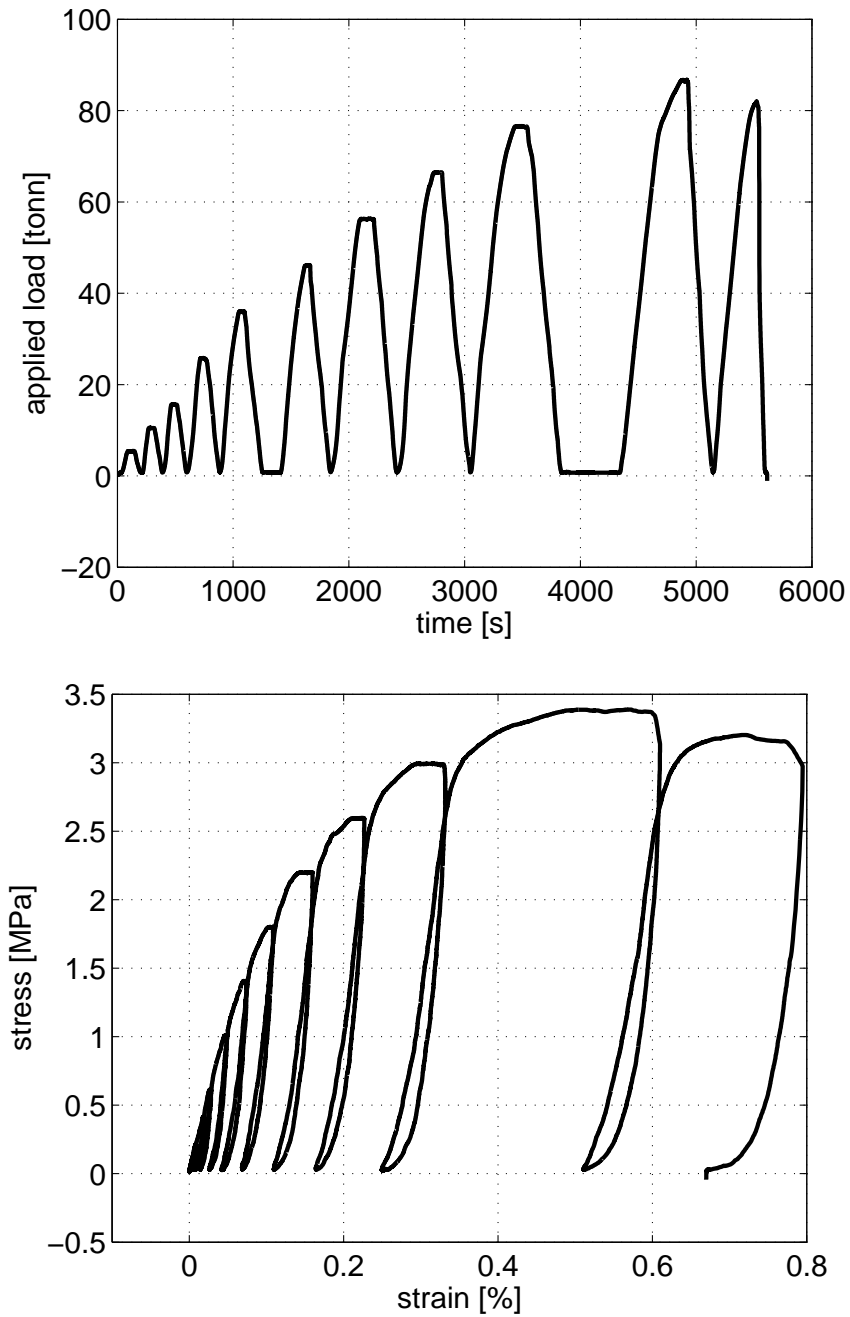
Figure 1.8: Upper side: applied load over time; Lower side:$\sigma - \varepsilon$ diagram

Table 1.4: Results of vertical compression tests

	f_m [MPa]	$\varepsilon\left(\sigma_{v,max}\right)$	$\sigma_{v,el}$	$\varepsilon\left(\sigma_{v,el}\right)$	E [MPa]
Mean	3.28	0.005	1.09	4.3E-4	2550
St. Dev.	0.26	0.0017	0.08	7.5E-5	345
C.o.V.	8%	34%	8%	17.4%	13.5%

	$\varepsilon_{vert}\left(\sigma_{v,el}\right)$	$\varepsilon_{hor}\left(\sigma_{v,el}\right)$	ν_{hor}	$\varepsilon_{transv}\left(\sigma_{v,el}\right)$	ν_{transv}
Mean	4.3E-4	8.1E-5	0.19	6.4E-5	0.15
St. Dev.	7.5E-5	4.1E-5	0.08	2.2E-5	0.03
C.o.V.	17%	51%	42%	34%	18%

1.2.2 Diagonal compression tests

The diagonal compression test is used to determine shear stiffness and strength of masonry. The ASTM and RILEM international standards present two possible interpretations of results.

Both standards state that if we consider a square homogeneous elastic masonry element, submitted only to shear stresses, the principal stresses at the middle of the panel will be inclined by $45°$ to the head and bed joint axes. One of the generated stresses is compressive, while the other is tensile. We assume that failure occurs when the principal tensile stress reaches the diagonal tensile strength of the masonry.
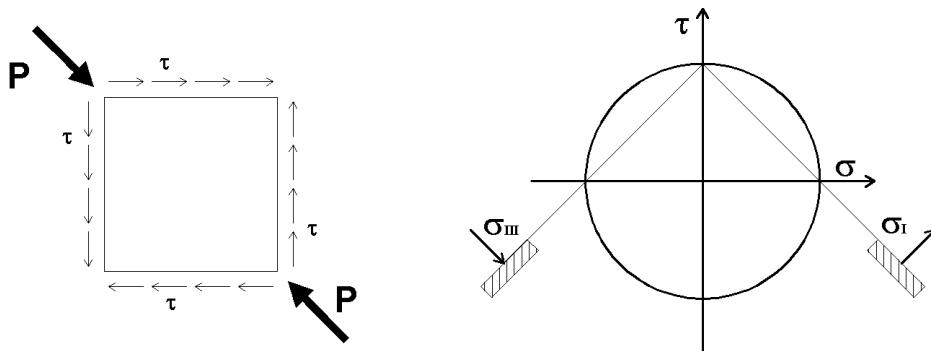
Figure 1.9: Tensional state stress from Mohr's circle (pure shear)

From the experiment point of view, shear stress is produced by the simultaneous presence of compression and tension along the diagonals of the specimens.

The following relation can hence be derived:

$$\tau_{xy} = \sigma_T = |\sigma_C| = \frac{P}{A_n\sqrt{2}} = 0.707 \cdot \frac{P}{A_n} \tag{1.8}$$

where A_n is the cross section area of the panel and P the acting load. When failure occurs, the tensile stress is equal to the strength of the material at the centre of the panel:

$$f_t = \sigma_T \tag{1.9}$$

Figure 1.10: Diagonal compression setup

The simplified hypothesis done is that in order to have a uniform distribution of tension on the panel, an additional tensile force equal to P should be applied to the other diagonal. Nevertheless, the real distribution of shear stresses is far from uniform and the panel is not subject to pure shear. ASTM and RILEM,

suggest a solution, that is widely used; the ultimate strength is then:

$$f_t = \frac{0.5 \cdot P_{max}}{A_n} \tag{1.10}$$

were A_n has already been defined, while P_{max} is the maximum acting load reached during the test.

The load was applied with the same compression machine describe in part 1.2.1. Figure 1.10 shows the test setup. For each specimen, 4 transducers where placed on both sides along the diagonal. The initial lengths of the transducers were highly variable, thus they were carefully measured before each test. The tests were performed for subsequent load cycles (table1.5), identified by increasing values of the tensile stress acting at the middle of the panel.

Table 1.5: Loading cycle and nominal average compression for diagonal compression tests

σ_T [MPa]	$Load$ [KN]
0.025	16
0.05	32
0.075	40
0.1	64
0.125	80
0.150	96
0.175	112
0.2	128
0.225	114
0.25	160

For each of the wall sides, the angular deformation γ can be derived as follow:

$$\gamma = \varepsilon_{vert} + \varepsilon_{hor} \tag{1.11}$$

where $\varepsilon_{vert} = {(\varepsilon_1 + \varepsilon_3)}/{2}$ and $\varepsilon_{hor} = {(\varepsilon_2 + \varepsilon_4)}/{2}$.

The shear modulus G in the elastic and post-elastic phase, can be determined. As for the vertical compression tests, the value of G (for the elastic range) was measured for the shear stress corresponding to one third of the maximum shear stress:

$$G = \frac{1/3 \cdot \tau_{max}}{\gamma(\tau_{el})} \qquad \text{where } \tau_{el} = 1/3 \cdot \tau_{max}$$

The results obtained from the tests are summarized in table 1.6. The stress-strain curve, corresponding to one of the performed tests (D4) and the applied load over time, are shown in 1.11 . The specimens showed a macroscopically linear behavior (constant slope of the curve) up to relatively high stress levels.

Table 1.6: Results of the diagonal compression tests

	τ_{max}^{ASTM}	f_t [MPa]	$1/3 \cdot \tau_{max}$	γ
Mean	0.197	0.137	0.065	7.96E-5
St. Dev.	0.043	0.031	0.015	2.45E-5
C. o. V.	21.8%	21.8%	21.8%	30.7%

1.2.3   Comments

The experimental tests described in this chapter provide the average value of some mechanical characteristics (table 1.7) needed for modeling structural elements under cyclic load and masonry building under dynamic tests.

Table 1.7: Summary of results

	f_m [MPa]	E [MPa]	f_t [MPa]	G [MPa]
Mean	3.28	2550	0.137	840
St. Dev.	0.26	345	0.031	125
C.o.V.	8%	13.5%	21.8%	14.8%

A scatter in the results can be observed, but it is limited with respect to compressive strength, while it is more evident for the Young's modulus. The largest variation is observed for the tensile strength obtained from diagonal compression tests. But this scatter is comparable to the one usually observed in tests on more regular and new masonry.

The results obtained from this experimental program were compared to the reference values provided by the Italian building code [20] to confirm that the masonry type used is classified as "undressed stone masonry with regular texture".
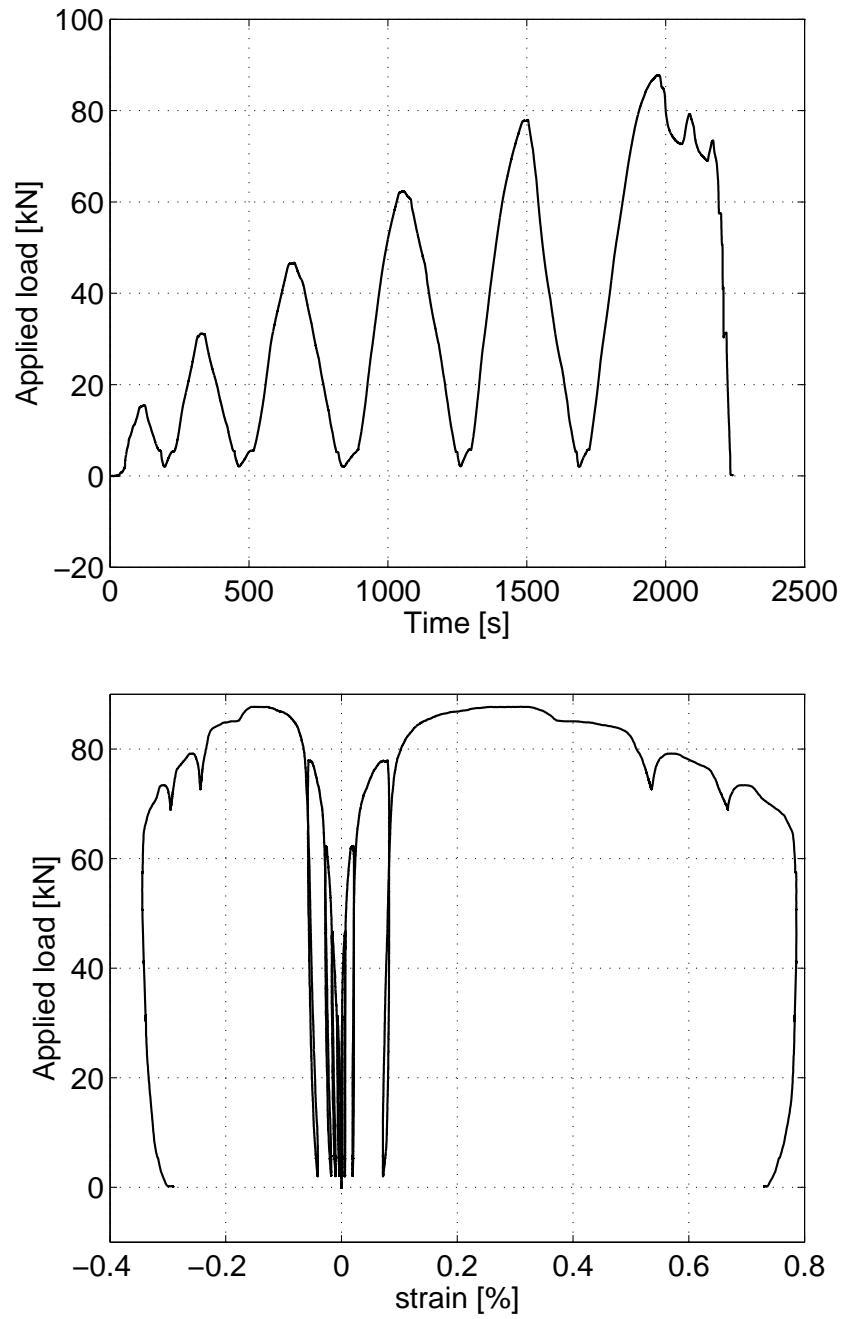
Figure 1.11: Diagonal compression

1.3   In-plane cyclic shear tests

With in-plane cyclic shear tests, the behavior of the wall subjected to reversal load is studied. The axial force imposed on the specimens represents the gravity loads, while the in-plane horizontal cycles simulate the seismic action. The information collected from these tests are: strength parameters, displacement capacity and hysteretic energy dissipation properties.

For the same specimen's dimensions, different failure modes take place, depending on the vertical axial compression:

- BENDING/ROCKING MECHANISM (in case of low compression): the damage is localized at the base and top cross sections and masonry deterioration is observed at the compressed toes (the compressive strength is locally exceeded);

- SHEAR FAILURE MODES: cracks develop along the compressed diagonal of the panel if the conventional tensile strength of the material is exceeded;

- HORIZONTAL CRACKS are governed by cohesion and friction and are usually observed along mortar joints.

The geometry of the specimens, the boundary conditions and the axial load applied were chosen in order to simulate a real wall of the 3D prototype. For this reason, all tests were performed in a double bending configuration. Moreover, two axial load ($0.5\,\mathrm{MPa}$ and $0.2\,\mathrm{MPa}$) and two slenderness ratios were taken into account. The specimens tested were:

- Squat: $2500 \times 2500 \times 0.32\,\mathrm{mm}$

- Slender: $2500 \times 1500 \times 0.32\,\mathrm{mm}$

1.3.1   Test setup and procedure

The cyclic in-plane tests were performed at EUCENTRE using the TREES Lab technology. There are three servo-hydraulic actuators, each having a maximum force capacity of $500\,\mathrm{kN}$; two of them apply the axial compression, while the
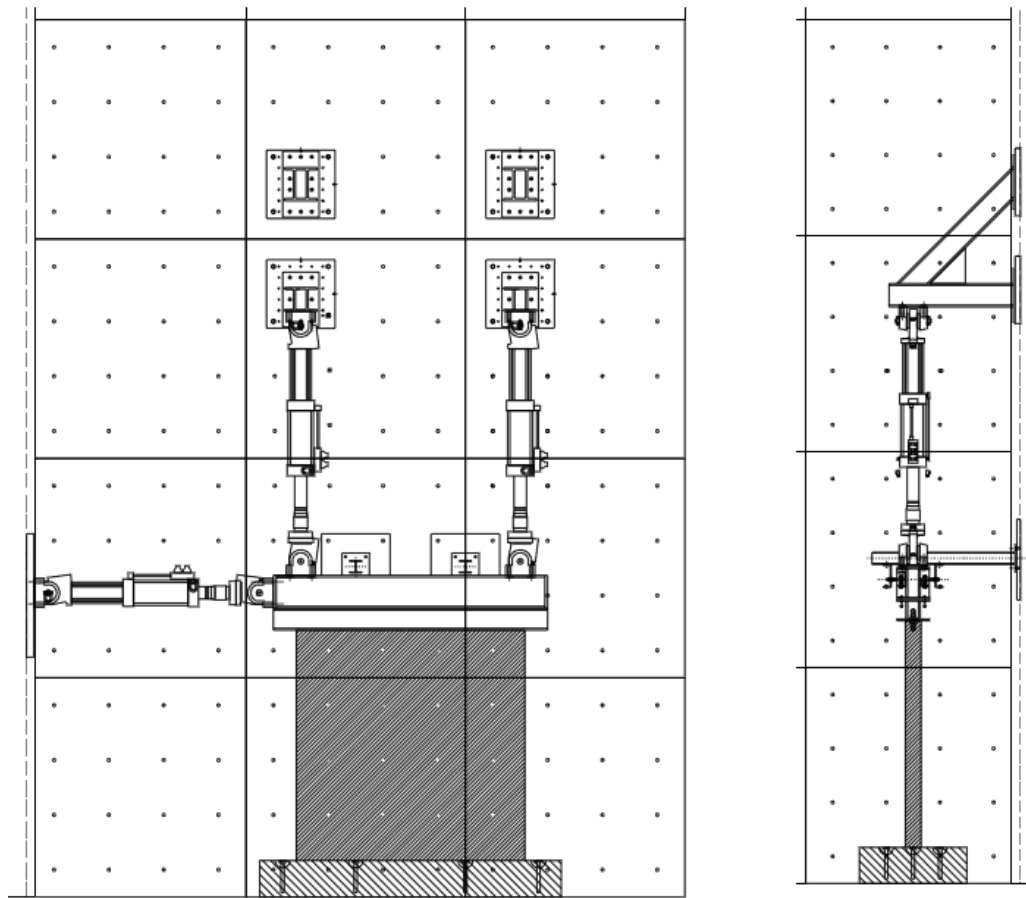
Figure 1.12: In-plane cyclic test: test setup

other imposes the horizontal displacements at the top of the specimen (figure 1.12).

Different restraint conditions can be imposed to the wall. A double bending configuration was chosen for all tests, thus the vertical rotation of the top steel beam was prevented by means of a "hybrid" control of the vertical actuators (they are forced to apply a constant total axial load and to maintain the same vertical displacement). This kind of control is automatically managed via software.

The procedure provides a first step in which the specimens are subjected to axial load only (80% of the value to be used during the test). The compression is then increased to reach the desired value to perform the test. During the second

phase of the test, the horizontal actuator is set in force control, and the specimen is subjected to a shear force equal to 1/4 of the shear strength estimated during complementary tests (described in part 1.2). The wall is firstly pushed and then pulled during a first sequence of loading called 1F. For the next sequence of three cycles (2F, 3F and 4F), the actuator is switched to displacement control with a target displacement equal to twice (2F), three times (3F) or four times (4F) that measured at cycle 1F. These cycles are characterized by a test velocity equal to $0.025\,\mathrm{mm/s}$.

The "D" set of cycles is a sequence of increasing target displacements corresponding to predefined values of drift, intended as the ratio between the horizontal displacement at the top and the wall height (table 1.8). If the drift to be applied at sequence 1D is less than those obtained for cycles 2F, 3F or 4F, these "F" cycles are skipped. The velocity of the actuator increases in proportion to the target displacement imposed.

The tests were stopped if the specimen presented potentially dangerous damage, a significant drop of lateral strength, or if the imposed drift reached the maximum capacity (3%) of the testing apparatus.

The axial load level chosen was decided with a preliminary numerical analysis of the reference full scale, two-storey prototype buildings and a maximum compression in the order of magnitude of $0.2\,\mathrm{MPa}$ was estimated. However, such a value is lower than the compressive strength of the material and lower than maximum compressive stress found in existing three or four storey buildings. This is due to the relatively small dimensions of the building prototypes subjected to shake table testing. Thus, it was decided to perform also tests with a higher level of applied compressive stress $(0.5\,\mathrm{MPa})$.

Four specimens, corresponding to the four combinations of parameters, were tested according to the procedure described above. The specimen named as CS00, built with a better quality mortar than the others, was tested with the purpose of a preliminary verification of the test setup.

Table 1.8: Summary of sequence

Sequence	Control	Velocity	Drift	Displacement [mm]
1F	force	(2.0-0.5) kN/s	(variable)	(variable)
2F	displ.	0.025 mm/s	(variable)	(variable)
3F	displ.	0.025 mm/s	(variable)	(variable)
4F	displ.	0.025 mm/s	(variable)	(variable)
1D	displ.	0.025 mm/s	±0.050%	±1.25
2D	displ.	0.038 mm/s	±0.075%	±1.875
3D	displ.	0.05 mm/s	±0.100%	±2.5
4D	displ.	0.065 mm/s	±0.150%	±3.75
5D	displ.	0.08 mm/s	±0.200%	±5
6D	displ.	0.1 mm/s	±0.250%	±6.25
7D	displ.	0.12 mm/s	±0.300%	±7.5
8D	displ.	0.16 mm/s	±0.400%	±10
9D	displ.	0.2 mm/s	±0.500%	±12.5
10D	displ.	0.24 mm/s	±0.600%	±15
11D	displ.	0.28 mm/s	±0.700%	±17.5
12D	displ.	0.32 mm/s	±0.800%	±20
13D	displ.	0.4 mm/s	±1.000%	±25
14D	displ.	0.5 mm/s	±1.250%	±31.25
15D	displ.	0.6 mm/s	±1.500%	±37.5
16D	displ.	0.7 mm/s	±1.750%	±43.75
17D	displ.	0.8 mm/s	±2.000%	±50
18D	displ.	1.0 mm/s	±2.500%	±62.5
19D	displ.	1.0 mm/s	±3.000%	±75

1.3.2 Results

The CS00 specimen, showed a flexural failure mechanism with no diagonal cracking, while for the other specimens collapse was always caused by diagonal cracks.

The CS02 specimen (low compression level) showed an initial phase of flexural damage, before reaching collapse in shear.

The two squat walls showed a clear shear failure, with cracks occurring along the diagonals of the specimens. No evidences of sliding was observed in any of the tests (possible sliding surfaces were monitored by transducers).

Figure 1.13: Specimen CS01

Figure 1.14: Specimen CT01

These experiments show that, for panels failed in shear, the ultimate shear resistance was approximately equal to the force at which the first visible diagonal crack appeared at the centre of the pier.

The shear strength associated with diagonal cracking can be expressed with the equation proposed by Tunseck and Sheppard [29]:

$$V_{res}^{diag-crack} = \frac{f_t \cdot l \cdot t}{b} \cdot \sqrt{1 + \frac{\sigma_0}{f_t}} \tag{1.12}$$

where

$$b = \begin{cases} 1.5 & h/l > 1.5 \\ h/l & 1 \le h/l \le 1.5 \\ 1 & h/l < 1 \end{cases}$$

f_t is the conventional diagonal cracking tensile strength of masonry;

σ_0 indicates the mean compressive stress acting on the pier;

l is the wall base;

t is the wall thickness.

When flexural failure occur, it is also possible to write an expression for the associated resistant shear force from the resistant moments which can develop at the top and base sections of the wall:

$$\begin{cases} M_{res}^{top} = \dfrac{\sigma_0^{top} \cdot t \cdot l^2}{2} \cdot \left(1 - \dfrac{\sigma_0^{top}}{0.85 \cdot f_m}\right) \\[2ex] M_{res}^{base} = \dfrac{\sigma_0^{base} \cdot t \cdot l^2}{2} \cdot \left(1 - \dfrac{\sigma_0^{base}}{0.85 \cdot f_m}\right) \\[2ex] V_{res}^{bending} = \dfrac{M_{res}^{top} + M_{res}^{base}}{h_{eff}} \end{cases} \tag{1.13}$$

where f_m is the compressive strength of masonry, "top" and "base" refer respectively to the top and base section of the wall. The assumption of constant compression along the height of the walls is not acceptable since a significant amount of the compression level is due to the self weight.

Tables 1.9 and 1.10 shows the values of tensile strength calculated from the measured maximum shear force by inverting equation 1.12. A good match can be observed between these values and those obtained from diagonal compression tests.

Table 1.9: Summary of cyclic tests on slender walls

Specimen	CS00	CS01	CS02
σ_0	$0.2\,\mathrm{MPa}$	$0.5\,\mathrm{MPa}$	$0.2\,\mathrm{MPa}$
Max Shear	49 kN	94 kN	48 kN
Last cycle	17D (2.0%)	9D (0.5%)	12D (0.8%)
failure	flexure	shear	flexure & shear
$f_{tu}\,[\mathrm{MPa}]$	—	0.16	0.10

Table 1.10: Summary of cyclic tests on squat walls

Specimen	CT01	CT02
σ_0	$0.5\,\mathrm{MPa}$	$0.2\,\mathrm{MPa}$
Max Shear	234 kN	154 kN
Last cycle	9D (0.5%)	10D (0.6%)
failure	shear	shear

Chapter 2

Modeling masonry: state of art

The purpose of this chapter is to describe how masonry can be modeled and the methods available in literature. Even though masonry is an ancient building technique, research in this field is very young and arose only in the last decades. The interest shown by the research community was open to advanced numerical tools, trying to separate masonry from its building tradition of trial and error.

The first attempt done by researchers was to import numerical tools available from more advanced fields, i.e. the mechanics of concrete. But such methods have proved useful to simulate masonry behavior only under certain condition. Thus, the particular features of masonry require appropriate tools to analyze structures built with this material.

Researches came up with several numerical models, based on different assumptions and characterized by different levels of detail. A unique model is not realistic because masonry structures differ in materials, texture and structural details. Analysts should choose the model that best suited his case, taking into account the information searched (serviceability, damage, collapse...), the accuracy required (local or global behavior), the input data needed (information about material) and finally, costs (that include, also the time needed to complete the analysis).

A division of all the methods implemented to model masonry is not available in literature, thus we decided to start from the classification proposed in [22].

2.1   Limit analysis

The simplest method used to describe masonry comes from the Mechanics of Solids and allows the study of the kinetics of collapse through the limit equilibrium analysis.

   With the basic assumptions of the method (which include no tensile strength and infinite compressive strength), the masonry panel can be modeled as kinematic chain of rigid blocks, described with the Lagrangian displacement magnitude at one point. Once suggested the failure mechanism, the system is reduced to an equivalent single degree of freedom (SDF) system where the horizontal static load factor can be calculated at the threshold of the system.

   With the assumption of rigid behavior until the establishment of linkage, the load factor represents the value (in g) of the horizontal acceleration at failure, associated to the mechanism suggested.

   The failure mechanisms can be divided into two types [8]. The mechanisms of first type relate to the out-of-plane behavior of masonry (out of plane bending and rocking.), while the mechanisms of second type include the in-plane behavior of the panel (shear and bending damage).

Figure 2.1: Possible failure mechanism in masonry panels (adapted from [8])
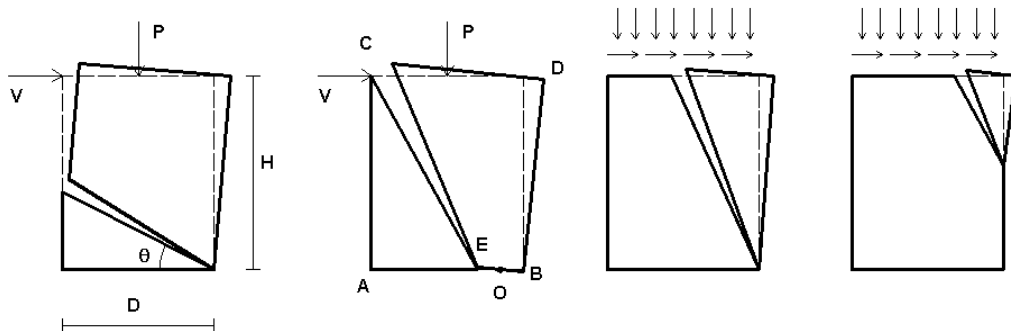
   With the aforementioned limit analysis method, the first failure mechanism is studied in an acceptable way, however, the second failure mechanism is assessed in an excessively precautionary way.

   Disadvantages of the method just described are that it does not take into account the elastic deformation of the structure and the post-elastic behavior; in

fact the strategy always leads to the study of equilibrium and kinematics of rigid bodies. Nevertheless, in the case of complex kinematics, the method has been very useful for evaluating the effects of consolidations.

An important application of the limit principles is the analysis of masonry arch [16]. Heyman's idea was that as most voussoir arches have low stresses and lines of thrust lie well within the masonry which mean that factors of safety have little relevance, thus a "geometrical" factor of safety may be defined. The geometrical factor considers the minimum thickness arch of the same shape as the real arch, which would just contain a proper line of thrust. This kind of analysis was applied to the stone arch between the western towers of Lincoln Cathedral and the Ponte Mosca in Turin and shows that the effect of geometry changes due to yielding of the abutments.

2.2   Equivalent strut

Another possibility for modeling masonry is the equivalent strut approach, which consider deformations in the elastic range possibly followed by inelastic deformation. Models which belong to this class may be bi-dimensional or mono-dimensional.
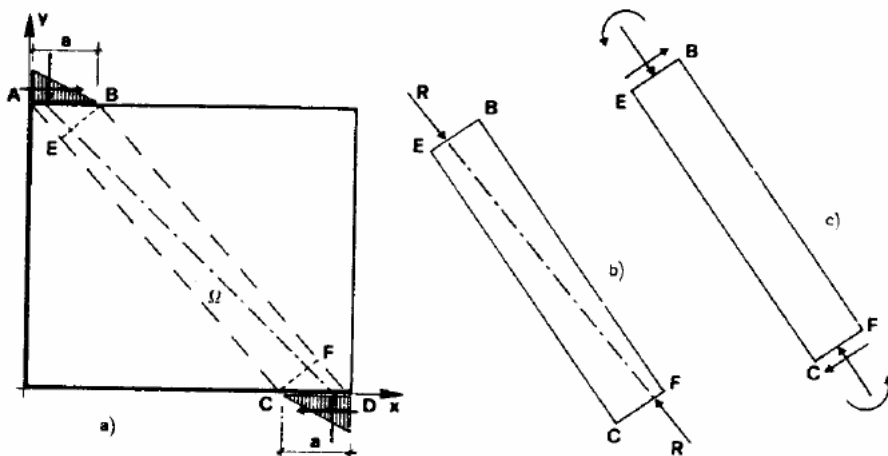

Figure 2.2: Masonry panel modeled through an equivalent strut [2]
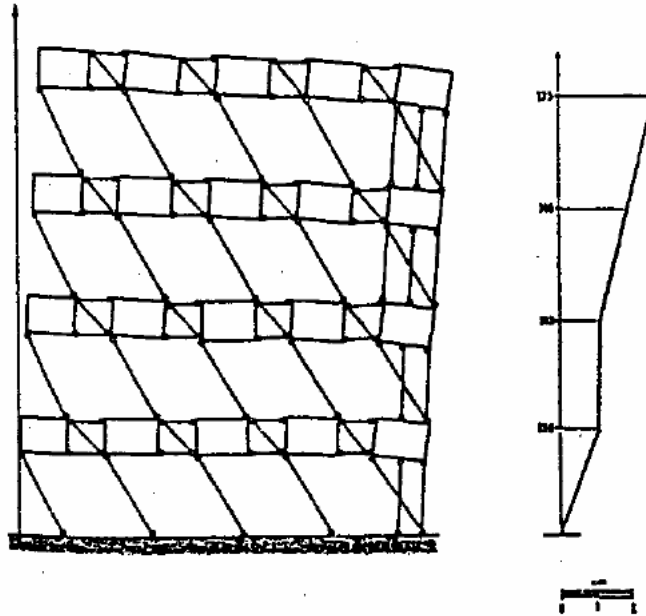
Figure 2.3: Masonry wall: equivalent strut [2]

Bi-dimensional approaches see masonry panels as equivalent elements with two main dimensions, while in a mono-dimensional approach, the masonry panel is divided into piers and lintels, regarded as equivalent struts. The connecting rod (strut) corresponds to the reactive part of the masonry panel, thus its inclination and its stiffness must reproduce the average behavior of the wall. Each panel can be in crisis if the equilibrium is not respected or cracks occur.

2.3 POR method

In 1978, Tomaževic proposed a method called POR [28]. At that time, computer where not so much widespread, so its first aim was to permit manual calculus to verify masonry structures. The method was based on the shear resistance of plain masonry walls failing, simulating story mechanism action of masonry buildings at ultimate state. The analysis of each story is done separately. Such approach greatly simplifies the accounts, but does not permit to consider the other possible failure modes.

Such method in his first version had several disadvantages:

1. The only part where deformations and cracks can occur are the piers. Other parts (lintels) are not considered places for possible damage.

2. The only possible failure mode is the shear one with diagonal crack. There is no presence of rocking and sliding.

3. Floors are considered rigid.

Several improvements were proposed to overcome the second problem, while the first and the third point have their limit inside.

Despite all the limitations mentioned before, the POR method has been greatly useful. Moreover, it is still a fundamental reference for Italian Code [20] for what concern the design of new buildings and the upgrading of old structures.

2.4 Macro-elements: equivalent models and frame models

With the approach of macro-elements, masonry panels are represent as a combination of structural elements (piers and lintels) as shown in figure 2.4.

The macro-elements approach needs low computational efforts because of the reduction of the degrees of freedom, but this method gives a rough description of the masonry elements. Usually, analysts choose the macro-elements approach when the object of the analysis is the global behavior of an entire structure (under cyclic loading).

An example of macro-element is the model proposed by Gambarotta and Lagomarsino [7]. Their approach (which was able to catch both overturning and hysteretic mechanism) has two degrees of freedom and was especially for rectangular masonry panels. Their work was then improved [1], and a non linear macro-element model was proposed. Figure 2.5 shows the macro-element; the structure is divided into three sub-structures. There are two layers (inferior and superior) where bending and axial effects are concentrate, while shear deformation are presented only in the central part.
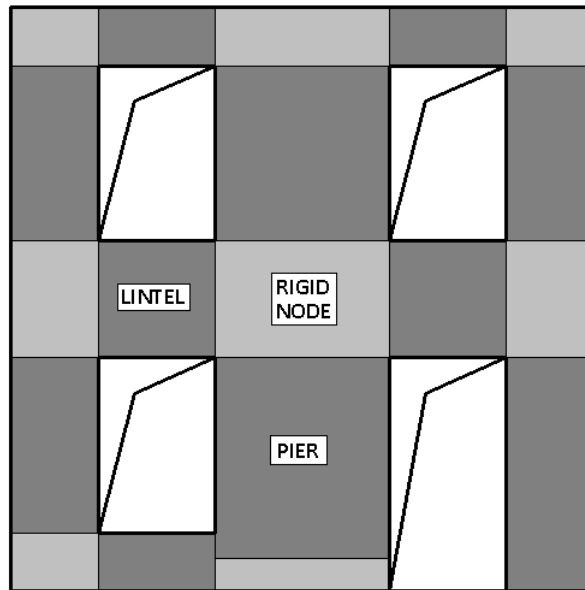
Figure 2.4: An example of macro-element modeling of a masonry wall

The element static and kinematic behavior is described with displacements, nodal rotations and resulting actions. Thus, it seems a mono-dimensional model, but the introduction of an internal degree of freedom gives to the element the ability to reproduce the behavior of masonry under cyclic load. For this reason, besides the need of a calibration of the material parameters, this method was very useful in research field as in practical applications.

Other important models that belong to the macro-element family are the ones classified as equivalent frames. An example of this sub-class is the SAM method [13].

SAM was developed at University of Pavia to analyze multistory walls with in-plane load and then improved for 3D problems.

As said before, the wall is divided into elements (piers and lintels) and rigid nodes, represented with offsets at the end of the elements. The piers height is determined with rules (proposed by Dolce [4]) which approximately take into account the deformation of the nodes; the lintels width in the model correspond to the real width of the lintels in the structure. The macro-element pier or lintel behavior is linear elastic up to the strength limit. Other important characteristics of the SAM method are:
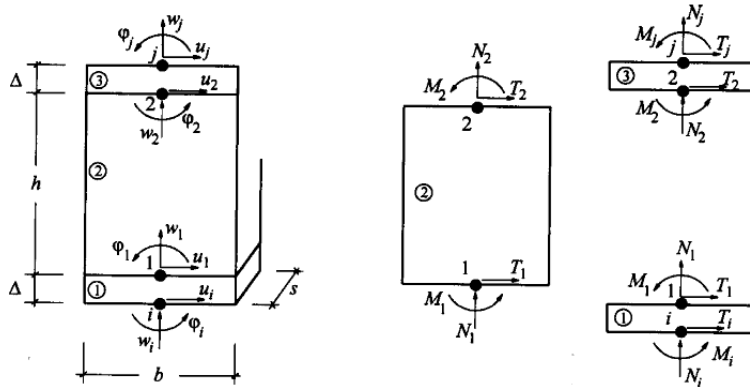
Figure 2.5: Kinematic model for the macro-element [1]

1. Lintels and piers are modeled as Timoshenko beam;

2. the frame strength is determined with the minimum strength criterion;

3. The displacement capacity of the frame depends on the expected failure mode.

The SAM method is valid and reliable to perform the push-over analysis of walls in 3D problems. The strength limit introduced depend on the axial compression of the piers at the single load step, thus they must be calculated with an iterative procedure.

2.5   Detailed models

There are methods that consider masonry as a composite material, focusing on the micro-modeling of each component (units and mortar) or on the macro-modeling of masonry as a composite. The aforementioned strategies refer to different fields of application: micro-models are applicable when the object of the study is the local behavior of the masonry, while macro-model are used when there must be a compromise between accuracy and efficiency. Anyway, both of these strategies need an exhaustive description of the material (usually done with an experimental program on masonry specimens).

Figure 2.7 shows three different ways of describing the material.
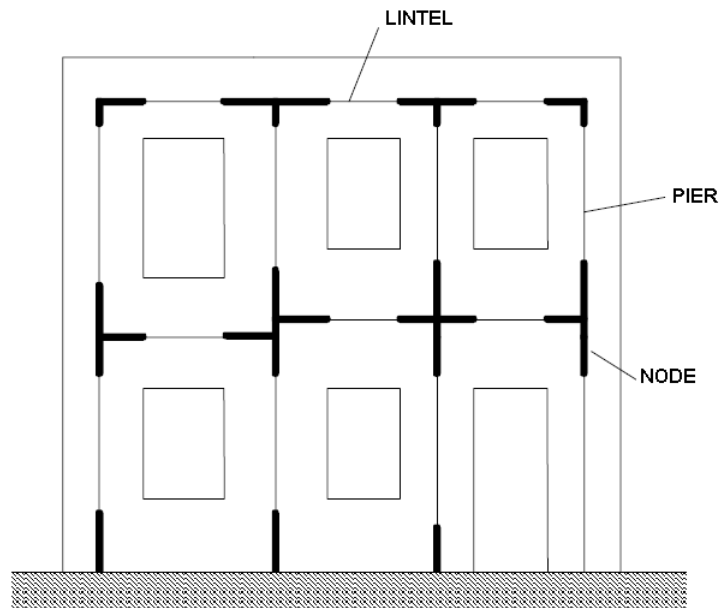
Figure 2.6: SAM method [13]

Micro-modeling There are two different kind of micro-model for masonry. In the *detailed micro-model*, continuum elements are used to describe units and mortar, while discontinuous elements are used to represent the unit-mortar interface. The behavior of both units and mortar is taken into account and the interface is a plane of potential crack. The aforementioned strategy is the most accurate model for describing masonry behavior, but requires a high computational effort. Thus, detailed mico-models are use only for an elaborated study of local response of masonry.

In the *simplified micro-modeling*, units are "expanded" and are modelled with continuum elements, while joints and unit-mortar interface are concentrated in discontinuous elements. In this way, units are directly bounded by potential fracture planes.

Both strategies have been developed for studying small elements with not homogeneous state of stress and strain. For this reason, input data comes from experimental laboratory tests on small samples.

32
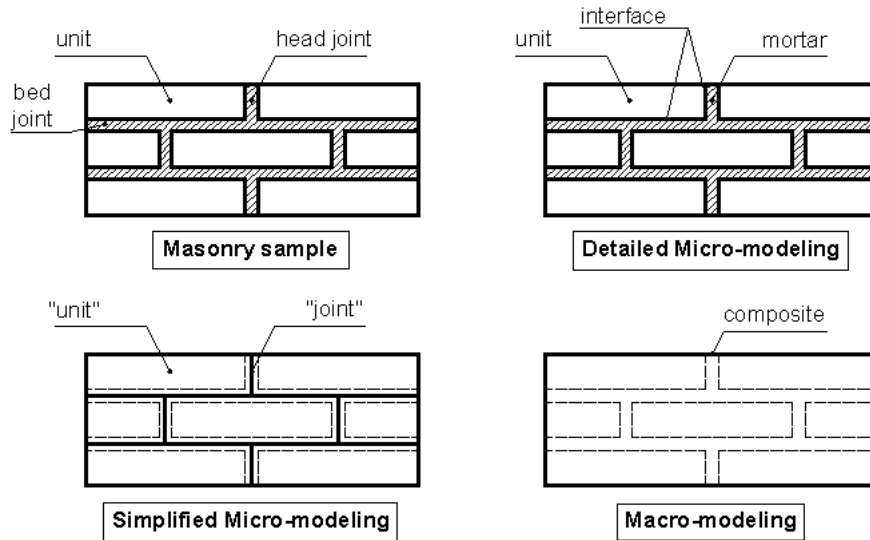
Figure 2.7: Modeling masonry (adapted from [10])

Macro-modeling (homogenization)   Everything (unit, mortar and their interface) is represented as a homogeneous anisotropic continuum. The macro-modeling approach is the most practice-oriented, due to its low computational request. This strategy needs an accurate description of the relationship between average stresses and average strains. Parametes, which describe the continuum, must be find out during tests on specimens (of large size) subjected to homogeneous state of stress.

Other advantages of macro-modeling include the fact that Finite Elements meshes are simpler, since the internal structure of the masonry is not described, and may not reproduce the masonry pattern. Moreover there are no complications with interfaces because homogeneous properties have been already calculated (with a micro-mechanical model).

Macro-models are used when the purpose of the research is the seismic behavior of old, complex, huge structures (i.e. bridges, cathedrals, historical buildings...)

An anisotropic plasticity model was proposed by Lourenço [10]. This implementation was (in its first formulation) suitable for modeling anisotropic materials under plane condition: he considered individual yield criteria for tension and

compression, according to different failure mechanism.

The compressive yield criterion (derived from Hill yield surface) was associated with a localized fractured process, while the tensile yield criterion (that refers to Rankine yield surface) is associated to a more distributed fracture process (figure 2.8)
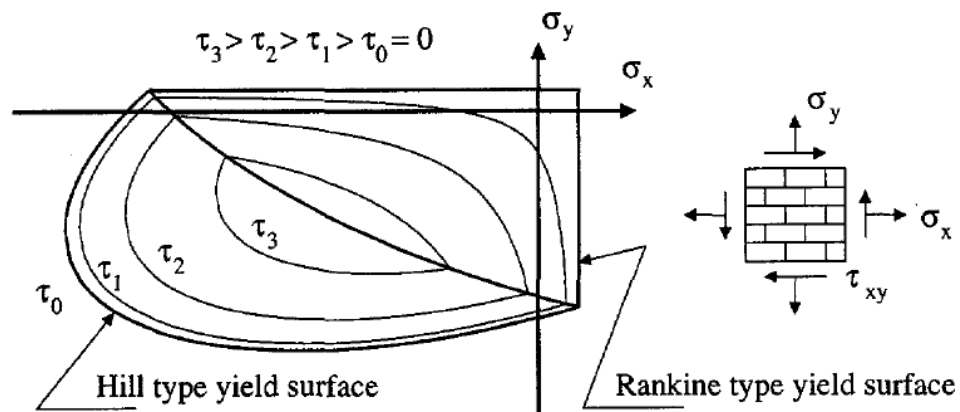
Figure 2.8: Lourenço's composite yield surface [10]

Another model was proposed by Gambarotta and Lagomarsino [6, 5] for modeling the seismic response of brick masonry. This model takes into account the mechanical behavior of each components and their interfaces (such as decohesion and slipping in mortar joints and faillure in bricks). The approach is suitable for the evaluation of the lateral response of in-plane loaded brick masonry shear walls.

The continuum model proposed is based on the assumption of an equivalent stratified medium made up of layers representative of the mortar bed joints and of the brick units and head joints, respectively. The constitutive equations are obtained through a homogenization procedure which involves the damage model of mortar joints [5] and simple damage constitutive equations for the brick layer.

This approach is used in finite element analysis of the in-plane response of brick masonry shear walls loaded either by cyclic horizontal actions superimposed on vertical loads or by dynamic loads, which are representative of the seismic actions. Validation tests were carried out and experimental results on squat and slender shear wall agree with numerical results.

34

Chapter 3

A commercial software: ABAQUS

This chapter describes the software used for the simulations of masonry behavior; the program chosen is Abaqus.

Abaqus is a finite element program that helps solving problems ranging from simple linear analyses to complex nonlinear simulations.

This code can solve problems that involve different elements modeled by associating the geometry and the material of each element and then choosing their interactions. In nonlinear analyses, load increments and convergence tolerances are chosen by the program; in this way Abaqus keeps on adjusting them to ensure that an accurate solution is obtained efficiently.

The Abaqus product suite, is made up of four core software:

1. Abaqus/CAE

2. Abaqus/CFD

3. Abaqus/Standard

4. Abaqus/Explicit

A complete Abaqus analysis consists of three distinct steps (pre-processing, simulation, and post-processing), as shown in figure 3.1.
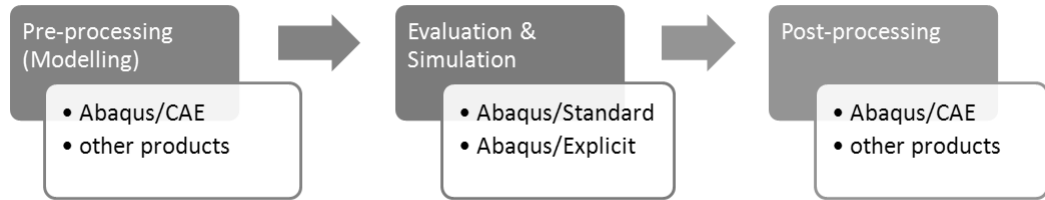
Figure 3.1: Abaqus software process

3.1 Pre-processing and Post-processing

Abaqus/CAE   Abaqus/CAE (Complete Abaqus Environment) is a Computer-Aided Engineering software application used in pre-processing (for design and modeling the components) and in post-processing (for visualizing the Finite element results).

The software is divided into modules that define a logical aspect of the modeling process. The modules are:

- *Part*: where the elements of the model are created.

- *Property*: materials and sections of each parts are defined

- *Assembly*: where the assembly is created and can be modified. Every model contains only one assembly, composed of instances of parts from the model.

- *Step*: where it is possible to create analysis steps and specify output requests.

- *Interaction*: where mechanical interactions (such as contacts) between regions is managed.

- *Load*: where loads and boundary conditions are defined.

- *Mesh*: where the mesh is generated.

- *Job*: where jobs are created and their progression is monitored.

- *Sketch*: where a sketch [1] is created.

- *Visualization*: where the output database is analyzed.

The model is build up by moving from module to module. When the model is completed, Abaqus/CAE generates the input file to be submitted to the Abaqus analysis product. The input file is read by Abaqus/Explicit or Abaqus/Standard and information are sent to Abaqus/CAE to allow the monitoring of the job progression. At the end of the job, the output database is generated and it can be read using the Visualization module in Abaqus/CAE.

Abaqus/CFD   Abaqus/CFD is a Computational Fluid Dynamics software application which is new to Abaqus 6.10.

This product is not used in this thesis, but it is here briefly described. It is very similar to Abaqus/CAE, but it provides more sophisticated computational fluid dynamics capabilities with extensive support for pre-processing and post-processing. With Abaqus/CFD it is possible to solve nonlinear coupled fluid-thermal and fluid structural problems.

3.2   Analysis procedures

The simulation is the stage in which Abaqus/Standard or Abaqus/Explicit solves the numerical problem defined in the pre-processing step. The analysis of the problem and its solution may take seconds or day, depending on the power of the computer and the number of variables.

Abaqus/Standard   Abaqus/Standard is able to solve a wide range of linear and nonlinear problems that involve either static or dynamic response of elements. Usually, models generated in Abaqus are nonlinear and can involve many variables.

---

[1]A sketch is a 2D profile used to help defining the geometry in Abaqus/CAE. A sketch might be extruded, swept, or revolved to form a 3D part.

Let $\mathbf{u}$ be the variable of the problem and $\mathbf{F}$ the force component, the problem is to find out the solution $\mathbf{u}$, solving the equilibrium equation below:

$$\mathbf{F}(\mathbf{u}) = \mathbf{0} \tag{3.1}$$

This problem is history-dependent, so the solution should be find for a series of "small" increments, using Newton's method. This numerical technique for solving nonlinear equilibrium equation, was chosen due to its better convergence rate compared to modified Newton or quasi-Newton method[2].

Newton's method says that after an iteration *i*, an approximation to the solution $\mathbf{u}_i$ is obtained. Let $\mathbf{c}_{i+1}$ be the difference between this solution and the exact solution of equation (3.1). This means that:

$$\mathbf{F}(\mathbf{u}_i + \mathbf{c}_{i+1}) = \mathbf{0} \tag{3.2}$$

Expanding this equation in Taylor series:

$$\mathbf{F}(\mathbf{u}_i) + \frac{\partial \mathbf{F}}{\partial \mathbf{u}}(\mathbf{u}_i)\mathbf{c}_{i+1} + \frac{\partial^2 \mathbf{F}}{\partial^2 \mathbf{u}}(\mathbf{u}_i)\mathbf{c}_{i+1}^2 + ... = 0 \tag{3.3}$$

Considering $\mathbf{u}_i$ as close approximation to the exact solution, the magnitude of each $\mathbf{c}_{i+1}$ will be small and so, all but the first two terms above can be neglected giving a linear system of equations:

$$\mathbf{K}_i \mathbf{c}_{i+1} = -\mathbf{F}_i \tag{3.4}$$

where $\mathbf{K}_i = \dfrac{\partial \mathbf{F}}{\partial \mathbf{u}}(\mathbf{u}_i)$ is the stiffness matrix and $\mathbf{F}_i = \mathbf{F}(\mathbf{u}_i)$.

As the iteration continues, the next approximation to the solution is then:

$$\mathbf{u}_{i+1} = \mathbf{u}_i + \mathbf{c}_{i+1}$$

If all entries in $\mathbf{F}_i$ and in $\mathbf{c}_{i+1}$ are small, convergence of the method is granted. This is checked by default in Abaqus/Standard solution.

---

[2]This is true for the types of nonlinear problems that are usually studied with Abaqus.

Newton's method needs to calculate the Jacobian matrix and solve linear equations at every single iteration . Thus, this method is computationally expensive.

Abaqus/Explicit   Abaqus/Explicit is able to solve problems that involve short, transient dynamic events (impact, blast, earthquake) and is also very efficient for highly nonlinear problems involving contact conditions.

This procedure is based upon the implementation of an explicit integration rule using diagonal or "lumped" element mass matrices. If the applied load vector $\mathbf{F}_i$ is known, the internal force vector $\mathbf{I}_i$ and the diagonal lumped mass matrix $\mathbf{M}$, the accelerations at the beginning of the increment are:

$$\ddot{\mathbf{u}}_i = \mathbf{M}^{-1} \cdot (\mathbf{F}_i - \mathbf{I}_i)$$

The problem is to find the dynamic equilibrium of the rigid body at the time t solving the equations below:

$$\dot{\mathbf{u}}_{i+\frac{1}{2}} = \dot{\mathbf{u}}_{i-\frac{1}{2}} + \frac{\Delta t_{i+1} + \Delta t_i}{2}\ddot{\mathbf{u}}_i$$

$$\mathbf{u}_{i+1} = \mathbf{u}_i + \Delta t_{i+1}\dot{\mathbf{u}}_{i+\frac{1}{2}}$$

where:

    $\mathbf{u}$ is the degree of freedom, displacement or rotation;

    $\dot{\mathbf{u}}$ is the velocity

    $\ddot{\mathbf{u}}$ is the acceleration

    i is the subscript that refers to the increment number in the dynamic analysis

    $i \pm \frac{1}{2}$ are the subscripts that refer to mid increment values.

Abaqus/Explicit is explicit because the kinematic analysis can process to that next increment knowing values of $\dot{\mathbf{u}}_{i-\frac{1}{2}}$ and $\ddot{\mathbf{u}}_i$ from previous increment.

This method is computationally efficient if the mass matrix of the problem is diagonal because its inversion is easier.

The explicit method does not require any iteration nor the calculus of the tangent stiffness matrix.

Stability   Using Abaqus/Explicit, the time incrementation scheme is automatic and does not required any user intervention.

The explicit procedure integrates through time by using many small time increments. Its stability is conditioned and the stability limit for the operator is given in terms of the highest eigenvalue in the system as:

- $\Delta t \leq {}^2\!/\!\omega_{max}$ neglecting dumping;

- $\Delta t \leq {}^2\!/\!\omega_{max} \cdot (\sqrt{1 + \xi^2_{max}} - \xi_{max})$ considering dumping (ξ is the fraction of critical damping in the highest mode).

Abaqus/Explicit contains a global estimation algorithm, which determines the maximum frequency of the entire model. This algorithm continuously updates the estimate for the maximum frequency. Abaqus/Explicit initially uses the element by element estimates. As the step proceeds, the stability limit will be determined from the global estimator once the algorithm determines that the accuracy of the global estimation is acceptable.

A conservative estimate of the stable time increment is given by the minimum taken over all the elements.

$$\Delta t = min \left(\frac{L_c}{c_d} \right)$$

where

L_c is the characteristic element dimension;

c_d is the current effective, dilatational wave speed of the material.

For beam, shell or membrane elements, the thickness of the element is not considered as the smaller dimension, but stability is referred to mid-plane.

Time increments must be minor than the stability limit. If this condition is not met, the solution of the problem would be instable.

Chapter 4

Material models and results

The core of this thesis is the material model for masonry and the study of its behavior under monotonic loading, cyclic loading and during in-plane cyclic shear tests. As already said in the Introduction, an "equivalent" masonry (homogenized material) was chosen, trying to use several material models already implemented in Abaqus. The choice was made after a rough classification of all possible material implementations available in Abaqus. We look for a material model:

1. able to describe different behavior in tension and compression;

2. with non-linear behavior in plastic branch;

3. possibly anisotropic[1].

It was not considered the progressive damage of the material, which means we do not consider the decreasing of Young's modulus during loading-unloading cycles.

The analyzed material models are described below, taking into account Abaqus Theory Manual [27] definition.

For each selected material model, several tests are performed to chose the parameters and check the accuracy of results proposed by the software:

1. uni-axial compression of a cube in force control and displacement control;

2. uni-axial tension of a cube in force control and displacement control;

---

[1]The intention is to find a material able to describe different behavior not in tension and compression, but also when the load direction changes.

3. uni-axial cycles in force control;

After that, the simulation of real tests done on masonry specimens is carried out. The tests implemented are:

1. vertical compression (in the direction normal to bed joints) of a jointed panel in force control;

2. diagonal compression of a panel in force control.

Finally, a comparison of the results produced with the different material models is presented.

4.1 Materials

4.1.1 Concrete damaged plasticity

The first choice is the concrete damaged plasticity model. The aforementioned model, implemented for both Abaqus/Standard and Abaqus/Explicit, provides a general capability for the analysis of concrete structures (but is suitable also for quasi-brittle materials) under cyclic and dynamic loading.

This constitutive theory wants to capture the irreversible effects of damage that occur in concrete under low confining pressure. To describe this behavior, the following features are considered:

1. the different yield strengths in tension and compression (with the initial yield stress in compression a factor of 10 or more higher than the initial yield stress in tension);

2. softening behavior in tension as opposed to initial hardening followed by softening in compression;

3. different degradation of the elastic stiffness in tension and compression;

4. stiffness recovery effects during cyclic loading;

5. rate sensitivity, especially an increase in the peak strength with strain rate.

The theory references of this implementation are the models propose by Lubliner [12] and by Lee and Fenves [9].

42

Strain rate decomposition   The rate independent model is governed by an additive strain rate decomposition:

$$\dot{\boldsymbol{\varepsilon}} = \dot{\boldsymbol{\varepsilon}}^{el} + \dot{\boldsymbol{\varepsilon}}^{pl}$$

where $\dot{\boldsymbol{\varepsilon}}$ is the total strain rate and the superscripts $'el'$ and $'pl'$ refer to the elastic and plastic part of the strain rate respectively.

Stress-strain decomposition   Stress-strain relations are:

$$\boldsymbol{\sigma} = \mathbf{D}^{el} : \left(\boldsymbol{\varepsilon} - \boldsymbol{\varepsilon}^{pl} \right) = \left(1 - d \right) \mathbf{D}^{el}_0 : \left(\boldsymbol{\varepsilon} - \boldsymbol{\varepsilon}^{pl} \right)$$

where $\mathbf{D}^{el}_0$ is the initial undamaged elastic stiffness of the material, $\mathbf{D}^{el}$ is the degraded elastic stiffness and d is the scalar stiffness degradation variable (undamaged material $d = 0$, fully damaged material $d = 1$). Hence, damage is represented with an isotropic reduction of the elastic stiffness with the scalar factor d.

Thus, the Cauchy stress is:

$$\boldsymbol{\sigma} = \left(1 - d \right) \bar{\boldsymbol{\sigma}}$$

where the effective stress $\bar{\boldsymbol{\sigma}}$ is define as $\bar{\boldsymbol{\sigma}} \overset{def}{=} \mathbf{D}^{el}_0 : \left(\boldsymbol{\varepsilon} - \boldsymbol{\varepsilon}^{pl} \right)$. When damage occurs, the effective stress $\bar{\boldsymbol{\sigma}}$ represent the effective stress area that is resisting the external loads. This is why it is better to formulate the plasticity problem in terms of $\bar{\boldsymbol{\sigma}}$.

Hardening variables   There are two different hardening variables: the equivalent plastic strain in tension $\tilde{\varepsilon}^{pl}_t$ and the equivalent plastic strain in compression $\tilde{\varepsilon}^{pl}_c$. Let $\dot{\tilde{\boldsymbol{\varepsilon}}}^{pl}$ the vector of the hardening variables, their evolution is defined as:

$$\dot{\tilde{\boldsymbol{\varepsilon}}}^{pl} = \mathbf{h} \left(\bar{\boldsymbol{\sigma}}, \dot{\tilde{\boldsymbol{\varepsilon}}}^{pl} \right) \cdot \dot{\boldsymbol{\varepsilon}}^{pl}$$

Besides micro-cracking and crushing, the hardening variables control also the evolution of the yield surface and the degradation of the elastic stiffness. Moreover

they are related to the fracture energy required to generate micro-cracks.

Under uni-axial condition it means that the stress curves have the form:

$$\sigma_t = \sigma_t \left(\tilde{\varepsilon}_t^{pl}, \dot{\tilde{\varepsilon}}_t^{pl}, \theta, f_i \right) \tag{4.1}$$

$$\sigma_c = \sigma_c \left(\tilde{\varepsilon}_c^{pl}, \dot{\tilde{\varepsilon}}_c^{pl}, \theta, f_i \right) \tag{4.2}$$

the subscripts $'t'$ and $'c'$ refer to tension and compression respectively;

$\dot{\tilde{\varepsilon}}_t^{pl}$ and $\dot{\tilde{\varepsilon}}_c^{pl}$ are the equivalent plastic strain ratios, while

$\tilde{\varepsilon}_t^{pl} = \int_0^t \dot{\tilde{\varepsilon}}_t^{pl} dt$ and $\tilde{\varepsilon}_c^{pl} = \int_0^t \dot{\tilde{\varepsilon}}_c^{pl} dt$ are the equivalent plastic strain in tension and compression;

θ is the temperature and

f_i $(i = 1, 2, ...)$ are other field variables.

The effective plastic strain rates under uni-axial loading conditions are given as:

$$\dot{\tilde{\varepsilon}}_t^{pl} = \dot{\varepsilon}_{11}^{pl} \ in \ uniaxial \ tension$$

$$\dot{\tilde{\varepsilon}}_t^{pl} = -\dot{\varepsilon}_{11}^{pl} \ in \ uniaxial \ compression$$

Let σ_c be as a positive quantities representing the magnitude of uni-axial compression stress, thus $\sigma_c = -\sigma_{11}$.

Starting from any point of the strain softening branch of the stress-strain curves, the response of the concrete specimen is weaker: the elastic stiffness of the material appears to be damaged (or degraded). The degradation of the elastic stiffness is significantly different between tension and compression tests (figure 4.1, figure 4.2), but either case show a more pronounced effect as the plastic strain increases. The concrete degradation is described through two independent variables d_t and d_c, which are increasing function of the equivalent plastic strain $\tilde{\varepsilon}^{pl}$, the temperature θ and field variables f_i:

$$d_t = d_t \left(\tilde{\varepsilon_t}^{pl}, \theta, \ f_i \right) \ \ 0 \leq d_c \leq 1 \tag{4.3}$$

$$d_c = d_c \left(\tilde{\varepsilon_c}^{pl}, \theta, \ f_i \right) \ \ 0 \leq d_c \leq 1 \tag{4.4}$$

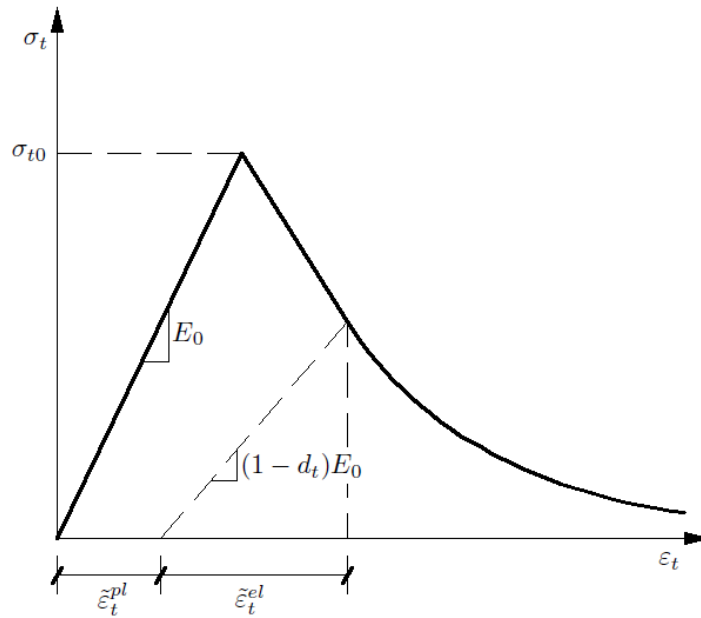Thus, let E_0 be the undamaged elastic stiffness, the stress-strain relations under

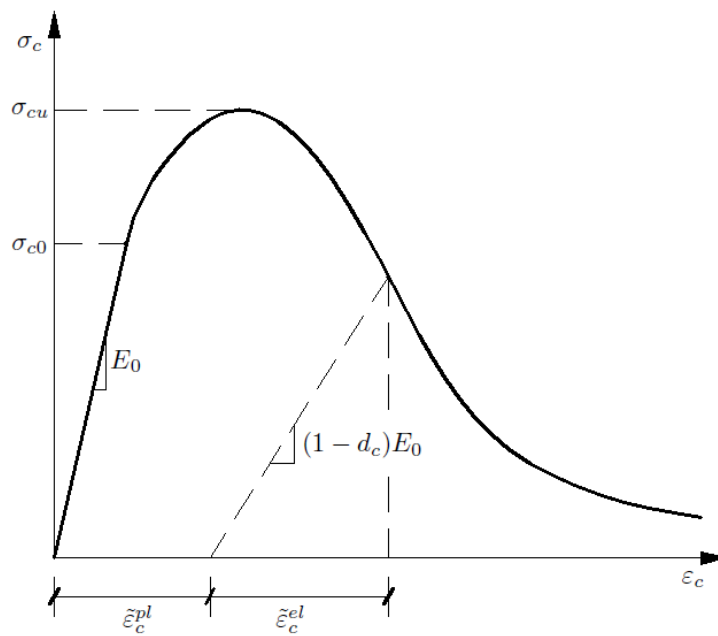Figure 4.1: Concrete response under uni-axial loading in tension

Figure 4.2: Concrete response under uni-axial loading in compression

uni-axial loading are:

$$\sigma_t = (1 - d_t) E_0 \left(\varepsilon_t - \tilde{\varepsilon_t}^{pl}\right) \tag{4.5}$$

$$\sigma_c = (1 - d_c) E_0 \left(\varepsilon_c - \tilde{\varepsilon_c}^{pl}\right) \tag{4.6}$$

The yield surface size is determined by the effective uni-axial cohesion:

$$\bar{\sigma}_t = \frac{\sigma_t}{(1 - d_t)} = E_0 \left(\varepsilon_t - \tilde{\varepsilon_t}^{pl}\right) \tag{4.7}$$

$$\bar{\sigma}_c = \frac{\sigma_c}{(1 - d_c)} = E_0 \left(\varepsilon_c - \tilde{\varepsilon_c}^{pl}\right) \tag{4.8}$$

Under uni-axial cyclic loading conditions the degradation involves the interaction of the micro-cracks that constantly open and close. The elastic stiffness recovers as the load changes sign and passes from tension to compression. Under such condition, the elastic modulus is given as a function of the undamaged modulus E_0 and the stiffness reduction variable d:

$$E = (1 - d) E_0$$

The stiffness reduction variable d is a function of the uni-axial damaged variables d_t and d_c:

$$(1 - d) = (1 - s_t d_c) (1 - s_c d_t)$$

where s_t and s_c represent the stiffness recovery effects associated to stress reversals:

$s_t = 1 - w_t \cdot r^*(\bar{\sigma}_{11})$; $s_t \geq 0$ and $0 \leq w_t \leq 1$

$s_c = 1 - w_c \cdot (1 - r^*(\bar{\sigma}_{11}))$; $s_c \leq 1$ and $0 \leq w_c \leq 1$

and

$$r^*(\bar{\sigma}_{11}) = H(\bar{\sigma}_{11}) = \begin{cases} 1 & if \ \bar{\sigma}_{11} > 0 \\ 0 & if \ \bar{\sigma}_{11} < 0 \end{cases}$$

The weight factors w_t and w_c describe material properties link to stiffness recovery. Figure 4.3 shows the default behavior used in Abaqus: the compressive stiffness is recovered upon crack closure as the load changes from tension to compression ($w_t = 0$), while the tensile stiffness is not recovered as the load

changes from compression to tension once crushing micro-cracks have developed $(w_c = 1)$.
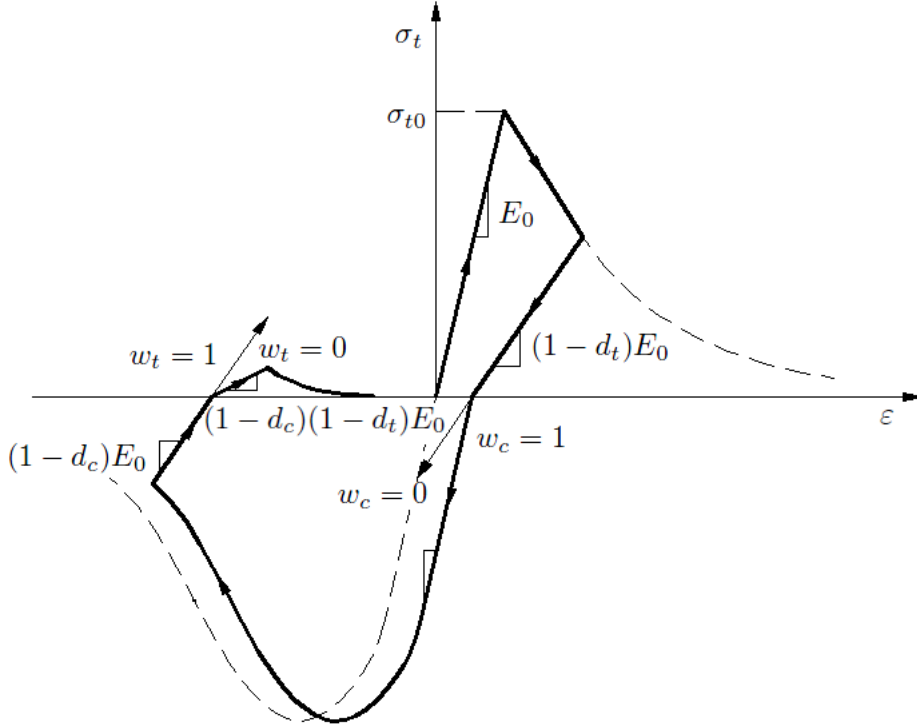

Figure 4.3: Uni-axial load cycle (tension-compression-tension) $w_t = 0$ and $w_c = 1$

Yield function The state of failure or damaged is represented, in the effective stress space, by the yield function:

$$F\left(\bar{\sigma}, \dot{\bar{\varepsilon}}^{pl}\right) \leq 0$$

The final form of the plastic-damage concrete model, takes into account different evolution of strength under tension and compression:

$$F\left(\bar{\sigma}, \dot{\bar{\varepsilon}}^{pl}\right) = \frac{1}{1-\alpha}\left(\bar{q} - 3\alpha\bar{p} + \beta\left(\dot{\bar{\varepsilon}}^{pl}\right)\left\{\hat{\bar{\sigma}}_{max}\right\} - \gamma\left\{-\hat{\bar{\sigma}}_{max}\right\}\right) \qquad (4.9)$$

where

$\bar{p} = -\frac{1}{3}\bar{\sigma} : \mathbf{I}$ is the effective hydrostatic pressure;

$\bar{q} = \sqrt{\dfrac{3}{2}\bar{\mathbf{S}} : \bar{\mathbf{S}}}$ is the Mises equivalent effective stress;

$\bar{\mathbf{S}} = \bar{p}\,\mathbf{I} + \bar{\boldsymbol{\sigma}}$ is the deviatoric part of the effective stress tensor $\bar{\boldsymbol{\sigma}}$;

$\hat{\bar{\sigma}}_{max}$ is the maximum eigenvalue of $\bar{\boldsymbol{\sigma}}$.

Let $\bar{\sigma}_c$ and $\bar{\sigma}_t$ be the effective tensile and compressive cohesion stresses, respectively, thus the function $\beta\left(\dot{\bar{\boldsymbol{\varepsilon}}}^{pl}\right)$ is:

$$\beta\left(\dot{\bar{\boldsymbol{\varepsilon}}}^{pl}\right) = \frac{\bar{\sigma}_c\left(\tilde{\varepsilon}_c^{pl}\right)}{\bar{\sigma}_t\left(\tilde{\varepsilon}_t^{pl}\right)}(1-\alpha) - (1+\alpha)$$

The coefficient α can be determined from the initial equi-biaxial and uni-axial compressive yield stress, σ_{b0} and σ_{c0}, as:

$$\alpha = \frac{\sigma_{b0} - \sigma_{c0}}{2\sigma_{b0} - \sigma_{c0}}$$

Typical values of α are between 0.08 and 0.12.

The Macaulay brackets are used to describe the ramp function:

$$\left\{\hat{\bar{\sigma}}_{max}\right\} = \begin{cases} 0, & \hat{\bar{\sigma}}_{max} < 0 \\ \hat{\bar{\sigma}}_{max}, & \hat{\bar{\sigma}}_{max} \geq 0 \end{cases} \text{ and } \left\{-\hat{\bar{\sigma}}_{max}\right\} = \begin{cases} 0, & \hat{\bar{\sigma}}_{max} \geq 0 \\ \hat{\bar{\sigma}}_{max}, & \hat{\bar{\sigma}}_{max} < 0 \end{cases}$$

thus, in bi-axial compression, when $\hat{\bar{\sigma}}_{max} = 0$, equation 4.9, reduces to the Drucker-Prager yield condition.

The coefficient γ enters in equation 4.9 only when the specimen is subjected to tri-axial compression and $\hat{\bar{\sigma}}_{max} \leq 0$ (typical value for concrete is $\gamma = 3$).

Figure 4.4, shows a typical yield surface in the deviatoric plane for plane-stress condition. It can be noted that besides all similarities that can be pointed out looking at the yield surface of figure 4.4 and Lourenço's yield criterion (figure 2.8), the Concrete Damaged plasticity model is not able to reproduce different behavior of the material when load changes direction.
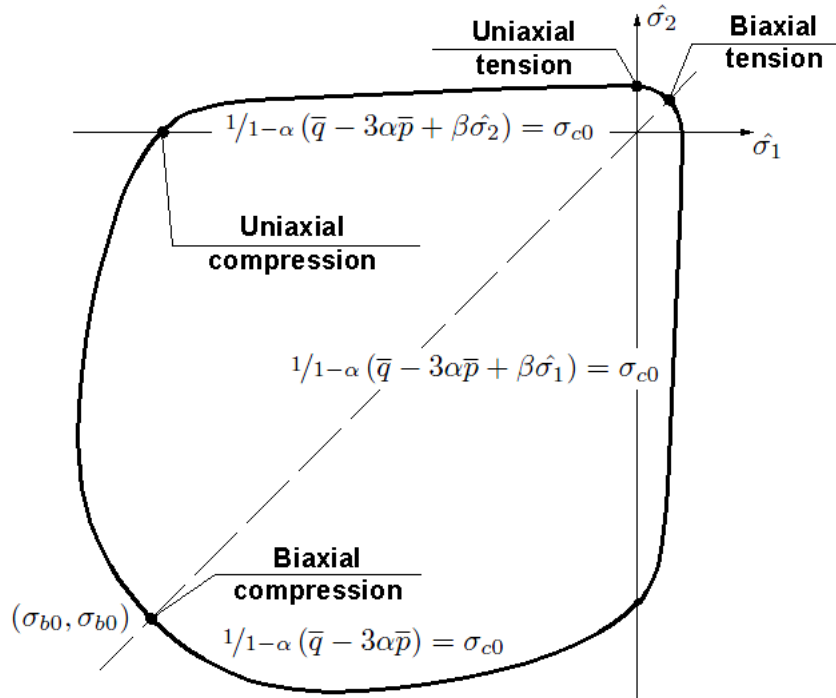
Figure 4.4: Yield surface in plane stress

Flow rule   The flow potential G governs the plastic flow with the flow rule, thus:

$$\dot{\bar{\varepsilon}}^{pl} = \dot{\lambda} \cdot \frac{\partial G\left(\bar{\sigma}\right)}{\partial \bar{\sigma}}$$

where $\dot{\lambda}$ is the non-negative plastic multiplier that obey, together with the yield function F, the Kuhn-Tucker conditions.

G is the Drucker-Prager hyperbolic function:

$$G = \sqrt{\left(\epsilon \cdot \sigma_{t0} \cdot tan\psi\right)^2 + \bar{q}^2} - \bar{p} \cdot tan\psi$$

where ψ is the dilation angle measured in the $p-q$ plane at high confining pressure, σ_{t0} is the uni-axial tensile stress at failure and ϵ is a parameter that describes the rate at which the function approaches its asymptote (the flow potential tends to a straight line as the eccentricity tends to zero). This flow potential, which is continuous and smooth, ensures that the flow direction is defined uniquely. The

49

function asymptotically approaches the linear Drucker-Prager flow potential at high confining pressure stress and intersects the hydrostatic pressure axis at 90°.

4.1.2   Concrete smeared cracking

The second material chosen was the concrete smeared cracking model, provided in Abaqus/Standard for plain concrete. Reinforced concrete can be modeled by using rebar elements, but their behavior is independent of the concrete behavior. This approach does not take into account the interaction between rebar and concrete, but there are some aspects able to reproduce this link in reinforced concrete (for example the "Tension Stiffening" option allow to simulates the load transfer across cracks).

This constitutive theory focuses mainly on cracking which is the most important aspect described and it occurs when stresses reach the "crack detection surface".

Other important features taken into account in the model are here briefly described:

1. The concrete behavior is intended for relatively monotonic loading under low confining pressure; the model neglects any permanent strain associated with cracking: cracks can close completely when the stress across them becomes compressive.

2. The model does not track individual macro-cracks, but it is intended to detect crack directions at a single constitutive calculation point. Once cracks appear at a point, the component forms of all vector and tensor valued quantities are rotated so that they lie in the local system defined by the crack orientation vectors and normal to the crack faces.

3. The model puts together a "compressive" yield surface (a simple Coulomb line written in terms of p and q) and a "crack detection" failure surface (that represent cracks that occur at a material calculation point in tension, figure 4.5).

However several concerns raised against such model. The most important is that the finite element results do not converge to a unique solution. Mesh sensitivity
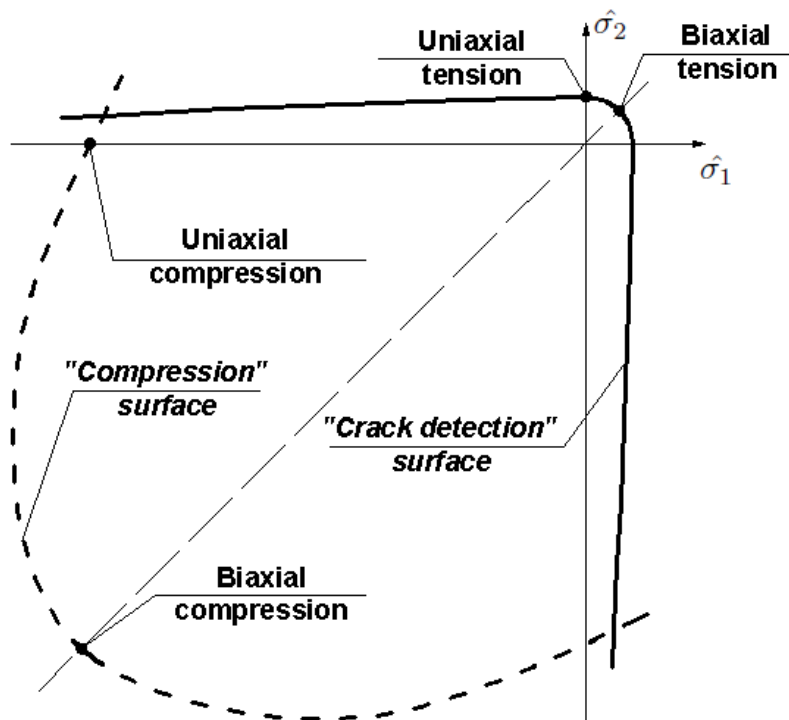
Figure 4.5: Concrete failure surfaces in plane stress

happens because the model simplifies the concrete behavior and the third stress invariant would be needed to improve this aspect of the material model.

Moreover, as already said for the concrete damaged plasticity model, also this material model is not able to reproduce different behavior of the material when load changes direction.

4.1.2.1 Elastic-plastic model

Strain rate decomposition The strain rare decomposition, associated to the compressive behavior is:

$$\dot{\varepsilon} = \dot{\varepsilon}^{el} + \dot{\varepsilon}^{pl}_c \tag{4.10}$$

where $\dot{\varepsilon}$ is the total mechanical strain rate, $\dot{\varepsilon}^{el}$ is the elastic strain rate (that includes crack detection strain) and $\dot{\varepsilon}^{pl}_c$ is the plastic strain rate related to the "compression" surface.

Compression yield function   The compression surface is defined by:

$$f_c = q - \sqrt{3} \cdot a_0 \cdot p - \sqrt{3} \cdot \tau_c = 0 \tag{4.11}$$

where

$p = -\dfrac{1}{3} \cdot Tr\left(\boldsymbol{\sigma}\right)$ is the effective pressure stress;

$q = \sqrt{\dfrac{3}{2}\mathbf{S} : \mathbf{S}}$ is the Mises equivalent effective stress;

$\mathbf{S} = p\mathbf{I} + \boldsymbol{\sigma}$ is the deviatoric part of the effective stress tensor $\boldsymbol{\sigma}$;

a_0 is a constant chosen from the ratio of the ultimate stress reached in bi-axial compression to the stress reached in uni-axial compression;

τ_c is a hardening parameter.

The constant a_0 depends on the user's data. In uni-axial compression, let σ_c be the stress magnitude, thus

$$p = \frac{1}{3} \cdot \sigma_c \text{ and } q = \sigma_c$$

therefore, on the yield surface $f_c = 0$:

$$\frac{\tau_c}{\sigma_c} = \left(\frac{1}{\sqrt{3}} - \frac{a_0}{3}\right) \tag{4.12}$$

Moreover, in bi-axial compression:

$$p = \frac{2}{3} \cdot \sigma_c \text{ and } q = \sigma_{bc}$$

where σ_{bc} is the magnitude of each nonzero principal stress, thus on the yield surface $\left(f_c = 0\right)$, it results that:

$$\frac{\tau_c}{\sigma_{bc}} = \left(\frac{1}{\sqrt{3}} - \frac{2a_0}{3}\right) \tag{4.13}$$

52

The a_0 constant can be easily calculated from equation 4.12 and equation 4.13

$$a_0 = \sqrt{3} \cdot \frac{1 - r_{bc}^\sigma}{1 - 2r_{bc}^\sigma} \tag{4.14}$$

where $r_{bc}^\sigma = \dfrac{\sigma_{bc}^u}{\sigma_c^u} \approx 1.16$.

Hardening variables   Hardening is defined by specifying the magnitude of the stress $|\sigma_{11}|$ in uni-axial compression tests as a function of the inelastic strain magnitude $|\varepsilon_{11}|$. The aforementioned data are used to define τ_c as follow:

$$\tau_c = \left(\frac{1}{\sqrt{3}} - \frac{a_0}{3} \right) \sigma_c \tag{4.15}$$

Flow rule   The model uses associated flow, so $\dot{\varepsilon}_c^{pl} = 0$ unless $f_c = 0$ and $\dot{\lambda}_c > 0$ and:

$$\dot{\varepsilon}_c^{pl} = \dot{\lambda}_c \left(1 + c_0 \left(\frac{p}{\sigma_c} \right)^2 \right) \frac{\partial f_c}{\partial \boldsymbol{\sigma}} \tag{4.16}$$

where c_0 is a constant chosen so that the ratio of $\left(\varepsilon_{11}^{pl} \right)_{bc}$ in a monotonically loaded bi-axial compression tests to $\left(\varepsilon_{11}^{pl} \right)_c$ in a monotonically loaded uni-axial compression tests is a value (r_{bc}^ε) specified by the user as part of the failure surface date (usually $r_{bc}^\varepsilon \approx 1.28$).

c_0 is derived from the user's definition of r_{bc}^ε, starting from the gradient of the flow potential for the compressive surface, thus:

$$\frac{\partial f_c}{\partial \boldsymbol{\sigma}} = \frac{\partial q}{\partial \boldsymbol{\sigma}} - \sqrt{3} \cdot a_0 \cdot \frac{\partial p}{\partial \boldsymbol{\sigma}}$$

Since

$$\frac{\partial p}{\partial \boldsymbol{\sigma}} = -\frac{1}{3} \mathbf{I} \text{ and } \frac{\partial q}{\partial \boldsymbol{\sigma}} = \frac{3}{2} \cdot \frac{\mathbf{S}}{q}$$

then, the gradient of the flow potential is:

$$\frac{\partial f_c}{\partial \boldsymbol{\sigma}} = \frac{3}{2} \cdot \frac{\mathbf{S}}{q} + \frac{a_0}{\sqrt{3}} \cdot \mathbf{I}$$

In uni-axial compression ($p = \frac{1}{3}\sigma_c$, $q = \sigma_c$ and $S_{11} = -\frac{2}{3}\sigma_c$), the integral of equation 4.16 gives:

$$\left(\varepsilon_c^{pl}\right)_{11}^c = \lambda_c \left(1 + \frac{c_0}{9}\right)\left(\frac{a_0}{\sqrt{3}} - 1\right)$$

while in bi-axial compression when both nonzero principal stresses have the magnitude σ_{b0} and

$$p = \frac{2}{3}\sigma_{bc} = \frac{2}{3} \cdot r_{bc}^\sigma \sigma_c \ , \ q = \sigma_{bc} = r_{bc}^\sigma \sigma_c \text{ and } S_{11} = -\frac{1}{3} \cdot r_{bc}^\sigma \sigma_c$$

the flow rule gives

$$\left(\varepsilon_c^{pl}\right)_{11}^{bc} = \lambda_c \left(1 + \frac{4}{9}(r_{bc}^\sigma)^2 c_0\right)\left(\frac{a_0}{\sqrt{3}} - \frac{1}{2}\right)$$

4.1.2.2   Crack detection

When the stress is predominantly tensile, cracking and post-cracking behavior are the most important aspects of the material implementation. The model take advantage of a "crack detection" plasticity surface in stress space to determine when cracking takes place and the orientation of the cracking. Then the post failure behavior of cracked concrete is described with damaged elasticity.

Numerically, the "crack detection" plasticity model is used for the increment in which cracking takes place, while, once the cracks presence and orientation have been detected, the damaged elasticity is used. When a crack is detected, its orientation is stored for subsequent calculations: subsequent cracks at the same point are restricted to being orthogonal to the first crack direction (thus no more than three cracks can occur) since stress components associated with an open crack are not included in the definition of the failure surface used for detecting the additional cracks. Cracks are not recoverable, but may open and close.

For the post-crack behavior, we assume that the fracture energy required to form a unit area of crack surface G_f is a material property and such a value can be calculated from measuring the tensile stress as a function of the crack opening displacement:

$$G_f = \int \sigma_t du$$

But, with this assumption, when the elastic part of the displacement u^{el} is eliminated, the relationship between the stress and the remaining part of the displacement $\left(u^{cr} = u^{tot} - u^{el}\right)$ is fixed, regardless of the specimen size. For this reason, the strain is multiplied by a characteristic length associated with the integration point. This characteristic crack length is based on the element geometry and formulation.

Strain rate decomposition   The elastic strain rate $\dot{\varepsilon}^{el}$ of equation 4.10 is decomposed as follow:

$$\dot{\varepsilon}^{el} = \dot{\varepsilon_d}^{el} + \dot{\varepsilon}_t^{pl}$$

where $\dot{\varepsilon_d}^{el}$ is the elastic strain rate and $\dot{\varepsilon}_t^{pl}$ is the plastic strain rate associated with the crack detection surface.

Yield function   The "crack detection" surface (Coulomb line) has a simple mathematical form but matches plane stress data quite well:

$$f_t = \hat{q} - \left(3 - b_0 \frac{\sigma_t}{\sigma_t^u}\right)\hat{p} - \left(2 - \frac{b_0\,\sigma_t}{3\,\sigma_t^u}\right) \tag{4.17}$$

where

σ_t^u \qquad is the failure stress in uni-axial tension

$\hat{q}\ and\ \hat{p}$ \qquad are defined in the same way as p and q, except that all stress components associated with open cracks are not included in these measures, but they are invariants in subspaces of the stress space.

b_0 \qquad is a constant.

The constant b_0 is function of the failure surface and is defined from the value of the tensile failure stress σ_I in a state of bi-axial stress when the other nonzero principal stress σ_{II} is at the uni-axial compression ultimate stress value σ_c^u

Flow rule   The crack detection model uses the assumption of associated flow, thus for $f_t = 0$ and $\dot{\lambda}_t > 0$,

$$\dot{\boldsymbol{\varepsilon}}_t^{pl} = \dot{\lambda}_t \frac{\partial f_t}{\partial \boldsymbol{\sigma}} \tag{4.18}$$

otherwise $\dot{\boldsymbol{\varepsilon}}_t^{pl} = 0$.

Hardening variables   Tension stiffening behavior is defined by introducing the magnitude of of the stress σ_t in uni-axial tension, when $S_{11} = \frac{2}{3}\sigma_t$ and $q = \sigma_t$. Equation 4.18 and equation 4.17 give, with the assumption of uni-axial tension:

$$\dot{\varepsilon}_t^{pl} = \dot{\lambda}_t \left(2 - \frac{b_0}{3} \cdot \frac{\sigma_t}{\sigma_t^u} \right)$$

Hence the $\sigma_t(\lambda_t)$ relationship is obtained from the tension stiffening input data by integrating the above equation.

4.1.2.3   Damaged elasticity

After crack is detected, the damaged elasticity is used to model the failed material. Let $\mathbf{D}$ be the elastic stiffness matrix, thus:

$$\boldsymbol{\sigma} = \mathbf{D} : \boldsymbol{\varepsilon}^{el}$$

Let α be a crack direction, the corresponding stress and strain are: $\sigma_{\alpha\alpha}$ and $\varepsilon_{\alpha\alpha}^{el}$. When cracks occur and $\varepsilon_{\alpha\alpha}^{open} > \varepsilon_{\alpha\alpha}^{el} > 0$, it results:

$$D_{\alpha\alpha} = \frac{\sigma_{\alpha\alpha}^{open}}{\varepsilon_{\alpha\alpha}^{open}}$$

where $\sigma_{\alpha\alpha}^{open}$ is the stress corresponding to $\varepsilon_{\alpha\alpha}^{open}$.

4.1.3   Extended Drucker-Prager

The Extended Drucker-Prager model was then studied. This family of model is suitable for frictional materials and is used when typical characteristics of granular materials are shown, such as:

1. Yield surface is independent from pressure and the material becomes stronger as the pressure increases;

2. Compressive yield strength is greater that the tensile yield strength;

3. Hardening and softening are isotropic;

4. Volume changes with inelastic behavior;

5. The material response is implemented for essentially monotonic loading.

This model needs linear elastic behavior if creep is defined, but in other cases the porous elastic model can be used too. Besides that, anisotropy can't be defined and it was already noticed that this aspect is important to model the diagonal tests and the in-plane cyclic tests.

4.1.4   Cast Iron Plasticity

The cast iron plasticity model was developed for constitutive modeling pf gray cast iron, which is more brittle than most metals. This brittleness is due to the micro-structure of the material which is a distribution of graphite flakes in a steel matrix. In tension the graphite flakes act as stress concentrators, leading to an overall decrease in mechanical properties (such as yield strength). In compression, on the other hand, the graphite flakes serve to transmit stresses, and the overall response is governed by the response of the steel matrix alone. Thus, the macroscopic characteristics of this material are:

1. different yield strengths in tension and compression, with the yield stress in compression being a factor of three or more higher than the yield stress in tension;

2. inelastic volume change in tension, but little or no inelastic volume change in compression;

3. different hardening behavior in tension and compression.

A Mises-type yield condition along with an associated flow rule models the material response under compressive loading, but this assumption is not true for tensile loading, then a pressure-dependent yield surface is required to model the brittle behavior in tension.

Even if this material model seems to be good for the "equivalent masonry", no trials were done to simulate the masonry behavior because this material, as all the other, does not allow to consider anisotropy, which is important to model the diagonal tests and the in-plane cyclic tests.

4.1.5 Porous Metal Plasticity

Another attempt has been made with the porous metal plasticity model. A preliminary study of the material was carried out, before starting the calibration of the model. The study revealed the fact that this model does not allow to model the different behavior in compression and tension.

The formulation is based on the yield condition suggests by Gurson:

$$F = \left(\frac{q}{\sigma_y}\right)^2 + 2 \cdot q_1 \cdot f \cdot \cosh\left(-\frac{3}{2} \cdot \frac{q_2 \cdot p}{\sigma_y}\right) - \left(1 + q_3 \cdot f^2\right) = 0 \qquad (4.19)$$

where

$p = -\dfrac{1}{3}\boldsymbol{\sigma} : \mathbf{I}$ is the effective pressure stress;

$q = \sqrt{\dfrac{3}{2}\mathbf{S} : \mathbf{S}}$ is the Mises equivalent effective stress;

$\mathbf{S} = p\mathbf{I} + \boldsymbol{\sigma}$ is the deviatoric part of the effective stress tensor $\boldsymbol{\sigma}$;

σ_y is the yield stress;

f is the fraction of the voids in the material;

q_1, q_2, q_3 are the coefficients of the void volume fraction and pressure terms.

Lets take the case of uni-axial tension where:

$$p = -\frac{1}{3} \cdot \sigma_{11} \text{ and } q = \sigma_{11}$$

equation 4.19 becomes:

$$F = \left(\frac{\sigma_{11}}{\sigma_y}\right)^2 + 2 \cdot q_1 \cdot f \cdot \cosh\left(\frac{3}{2} \cdot \frac{q_2}{\sigma_y} \cdot \frac{1}{3} \cdot \sigma_{11}\right) = C \qquad (4.20)$$

where $C = (1 + q_3 \cdot f^2)$.

The hyperbolic cosine is an even function and in this case is summed to a always positive quantity, thus the difference in behavior related to the sign of σ_{11} is minimum.

For this reason, the porous metal plasticity model has been rejected and no simulation where done with this implementation.

4.2   Discussion of results

As already said at the beginning of this chapter, for each material chosen, several tests are performed to chose the parameters and check the accuracy of results proposed by the software. Tests run for calibration are:

1. uni-axial compression of a cube in force control and displacement control;

2. uni-axial tension of a cube in force control and displacement control;

3. uni-axial cycles in force control.

For some parameters, these tests are not enough for a good calibration as different values do not change the material behavior: in these cases calibration is concluded with the first test on the jointed specimen.

After the first step, the simulation of real tests done on masonry specimens is carried out. The tests implemented are describe in section 4.2 and are:

1. vertical compression (in the direction normal to bed joints) of a jointed panel in force control;

2. diagonal compression of a panel in force control.

If the simulations lead to satisfactory results, the simulation of in plane cyclic test is performed and finally, a comparison of results produced with different material is done [2].

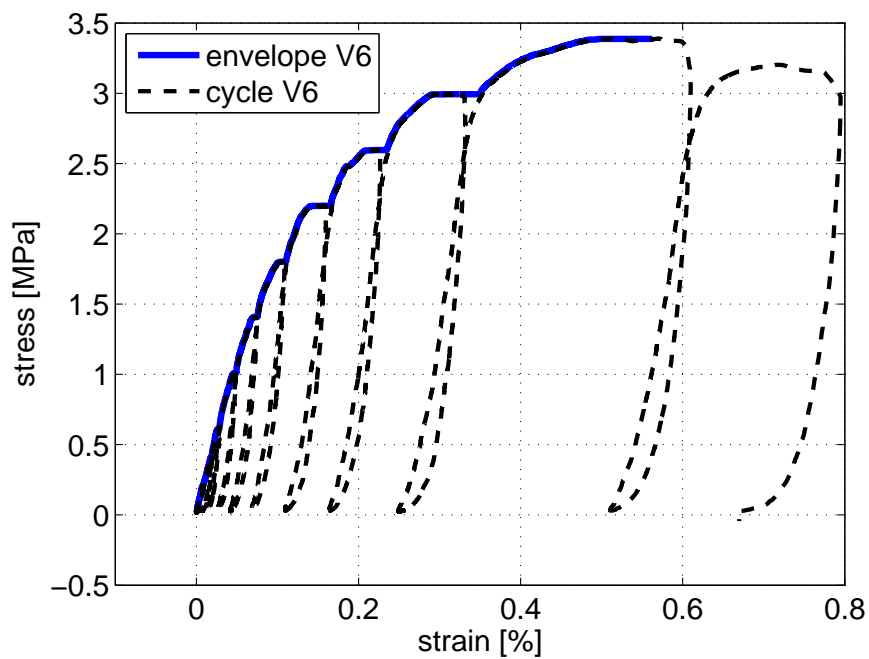The reference $\sigma - \varepsilon$ diagram for the compression tests comes from the sixth specimen proved in the vertical compression test (figure 4.6).

Figure 4.6: Reference $\sigma - \varepsilon$ diagram

---

[2]During these simulations the element used are C3D8R, that means 8-node linear brick, reduced integration, hourglass control (for more details see [23])

4.2.1   Concrete damaged plasticity

The concrete damaged plasticity model is described in part 4.1.1. Here, the parameters needed to define the concrete damaged plasticity model are analyzed; the following data need to be characterize:

1. Dilation angle: ψ (in degrees) in the p–q plane.

2. Eccentricity: ϵ a small positive number that defines the rate at which the hyperbolic flow potential approaches its asymptote (default $\epsilon = 0.1$)

3. fb0/fc0: that is σ_{b0}/σ_{c0}, the ratio of initial equi-biaxial compressive yield stress to initial uni-axial compressive yield stress (default $\sigma_{b0}/\sigma_{c0} = 1.16$)

4. K: K_c must satisfied the yield condition, thus $0.5 < K_c < 1$ (default $K_c = {}^2/_3$)

5. Viscosity Parameter: μ is used for the visco-plastic regularization on the constitutive equation in Abaqus/Standard analysis (default $\mu = 0.0$)

The values used for the first analysis are the default ones. If a parameter is unknown, starting from the default value, some tests are performed to see how the stress-strain diagram changes. Table 4.1 shows the parameters picked for the first compression test and table 4.2 the ones chose after calibration.

Table 4.1: Parameters (first test)

ψ	ϵ	σ_{b0}/σ_{c0}	K_c	μ
37°	0.1	1.16	0.67	0.0

Table 4.2: Parameters (after calibration)

ψ	ϵ	σ_{b0}/σ_{c0}	K_c	μ
47°	0.1	1.00	0.51	0.0
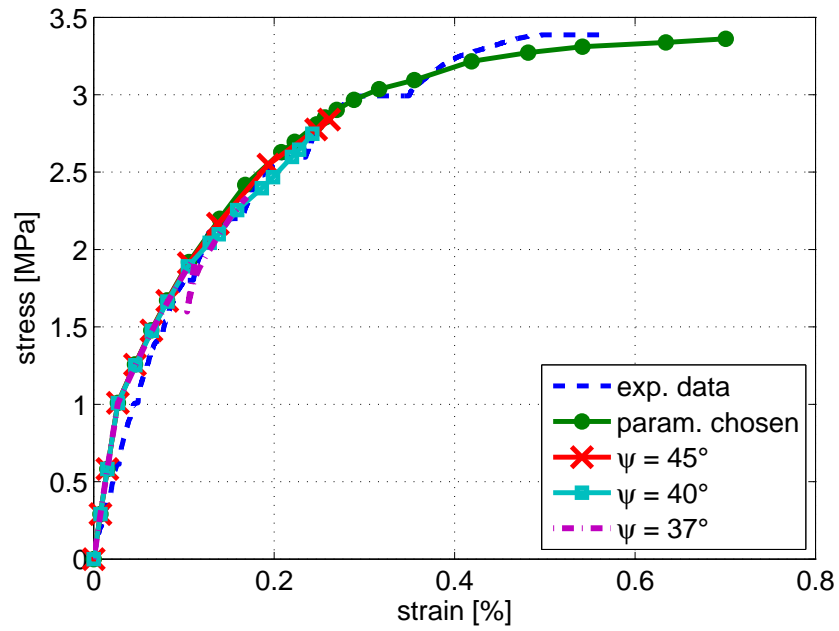
Figure 4.7: Comparison for different value of ψ
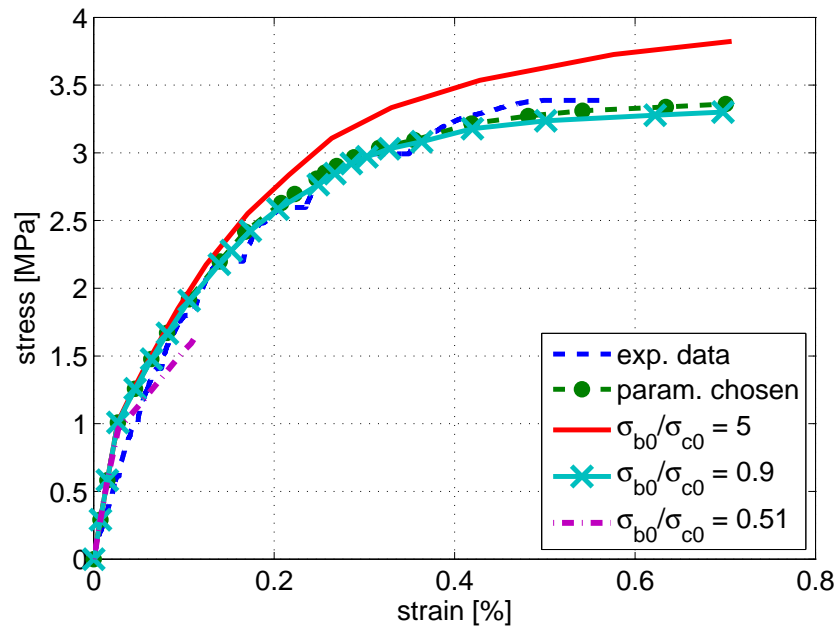
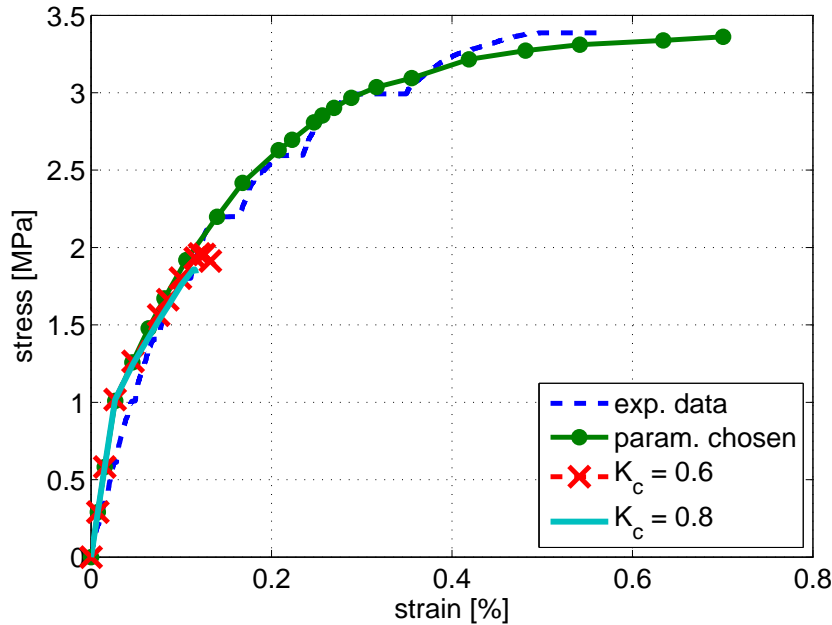Figure 4.8: Comparison for different value of σ_{b0}/σ_{c0}

Figure 4.9: Comparison for different value of K_c

Tests shown in figures 4.7, 4.8, 4.9 are carried out for a jointed specimen, to see how different parameters value can change the "equivalent masonry" behavior. In all diagrams only one parameter is made to vary while others are kept fixed.

Moreover the "compressive behavior" and the "tensile behavior" have to be defined.

The compression behavior outside the elastic range is defined with a tabular function of stress σ_c over the inelastic deformation $\tilde{\varepsilon}_c^{in}$ (see figure 4.10). Abaqus automatically converts the inelastic strain values to plastic strain values.

If we define the elastic strain:

$$\varepsilon_{c0}^{el} = \frac{\sigma_c}{E_0}$$

through the relationship:

$$\tilde{\varepsilon}_c^{in} = \varepsilon_c - \varepsilon_{c0}^{el}$$

63

the plastic strain value is obtained:

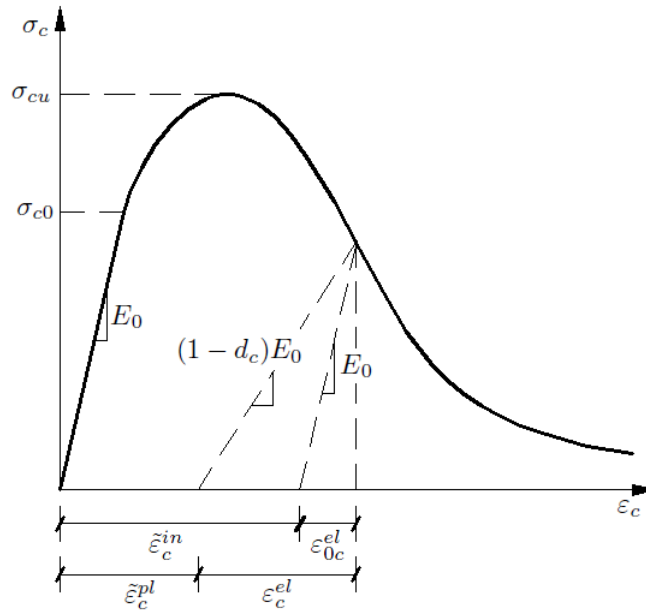$$\tilde{\varepsilon}_c^{pl} = \tilde{\varepsilon}_c^{in} - \frac{d_c}{(1-d_c)} \cdot \frac{\sigma_c}{E_0}$$

Figure 4.10: Definition of compressive inelastic strain

Table 4.3: Compressive behavior

Yield Stress [MPa]	Inelastic strain
1.05	0
1.50	0.000261
2.13	0.000696
2.60	0.001172
2.94	0.001981
3.25	0.002524
3.31	0.003379
3.39	0.004254
3.38	0.004555
3.34	0.004864
3.31	0.005064

Table 4.3 describe the tabular data introduced in Abaqus to define the compressive behavior of the material model used.

The tensile behavior after crack can be defined in two different ways. The first one defines the post-failure behavior giving the post-failure stress σ_t as a function of cracking strain $\tilde{\varepsilon}_t^{in}$ (as happens in compression.). Figure 4.11 shows the definition of $\tilde{\varepsilon}_t^{in}$. This kind of approach introduces mesh sensitivity in case of no reinforcement. Thus, as masonry is without reinforcements, its tensile behavior after cracks is defined as a function of the fracture energy G_f required to open a unit area of crack.

Under tension a concrete specimen will crack across some section. The cracks opening do not depend on the specimen's length. The post-failure stress can be defined as a tabular function of cracking displacement or of the associated fracture energy. This last model assumes a linear loss of strength after cracking (figure 4.12).
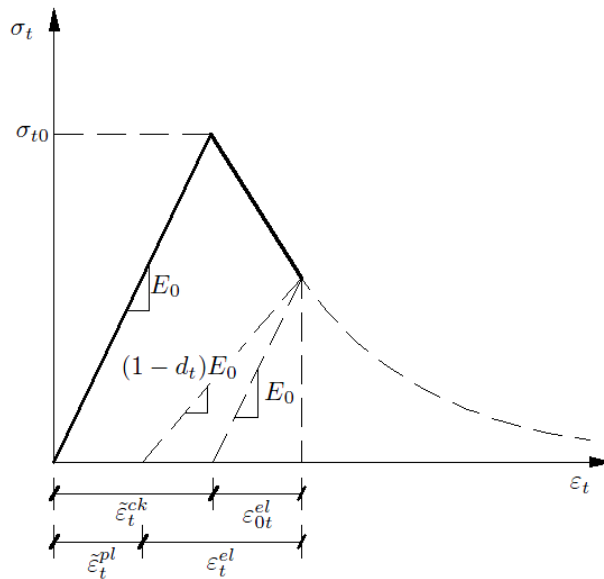

Figure 4.11: Definition of tensile inelastic strain

A typical value of G_f for unreinforced concrete is $40\,\mathrm{N/m}$, thus for masonry, a value ranging between $5\,\mathrm{N/m}$ and $10\,\mathrm{N/m}$ was taken into account.

Nevertheless, despite this definition of tensile behavior, some mesh sensitivity remains. The model requires a characteristic length (based on the element geometry and formulation) associated with an integration point; the characteristic crack length is automatically decided by the software.
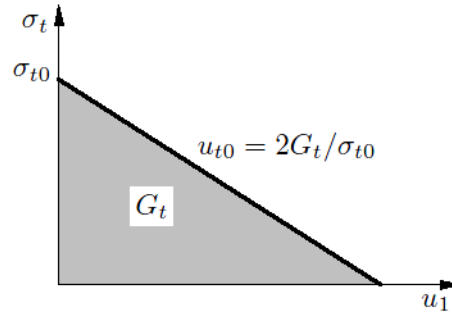

Figure 4.12: Post-failure stress-fracture energy curve

Damage is defined through d_t and d_c which are defined in part 4.1.1 and can be specified in tabular form, but in this case they are not required.

As already discussed in part 4.1.1, the stiffness recovery is an important aspect of concrete definition. In this case, the behavior of masonry correspond to the default condition in Abaqus; it means that $w_t = 0$ and $w_c = 1$ (as already shown in figure 4.3).

The elastic properties must be defined to run the analysis: the Young's modulus find out during the experimental tests was $E = 2550\,\mathrm{MPa}$, but to better simulate the masonry behavior a new modulus was used. The new stiffness is:

$$E_{new} = 1.5 \cdot E = 3825\,\mathrm{MPa}$$

The Poisson's ratio introduced is $\nu = 0.19$.

The first implemented tests are carried out under uni-axial condition. Figure 4.13 shows a comparison, for the test of uni-axial compression of a cube, between force and displacement control. The diagram shows also the envelope of the $\sigma - \varepsilon$ trend for the sixth specimen. It must be said that the parameters chosen well simulate the behavior expected in compression under uni-axial condition.

66

For what concern the behavior in tension, no data are available. Figure 4.14 shows a comparison between force and displacement control in a uni-axial tension test of a cube.

Figure 4.15 represent the comparison between the experimental results and the numerical Abaqus results for a cube under uni-axial cycles in force control (Table 4.4). Even for cyclic load, Abaqus can follow masonry's behavior. Tests in force control aborted at the maximum value of σ is reached, while in displacement control the post-peak behavior is observed.

Uni-axial tests do not represent the real boundary condition of the specimen. Thus, more tests are done on specimen of the same dimension of the one describe in Chapter 1 subjected to vertical compression. With a jointed base, the material behavior changes. Figure 4.16, shows the behavior of the material implemented (in a compression test drove both in displacement and force control) compared to the expected behavior. As for uni-axial tests, simulations run in force control aborted as the maximum value of σ is achieved. The "General, Static" procedure does not allow to follow the $\sigma - \varepsilon$ diagram. A "Risk, Static" procedure is needed, but with this type of analysis, no loading cycles are permitted.
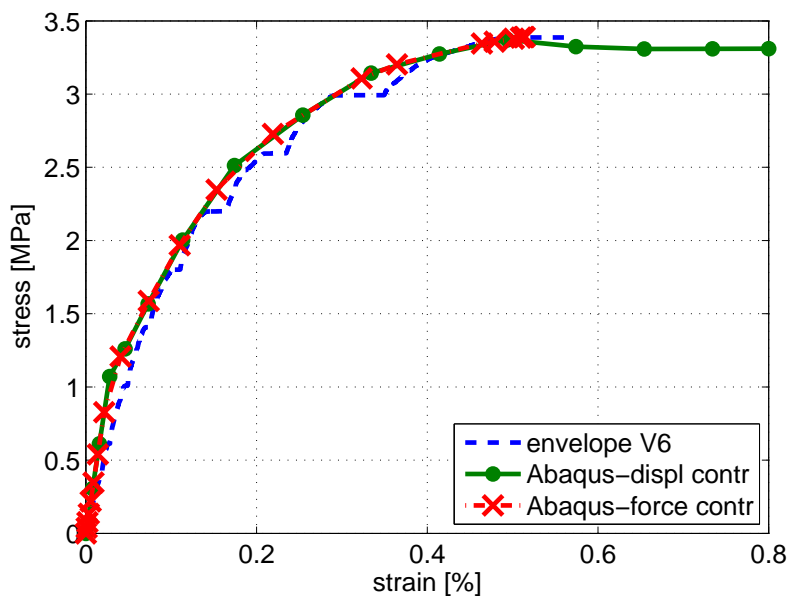

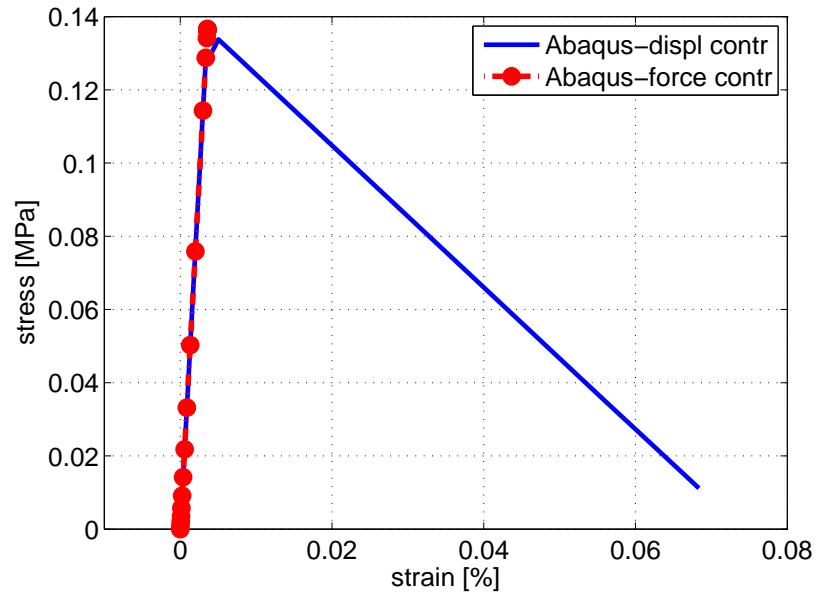Figure 4.13: Comparison between experimental and numerical data in uni-axial compression

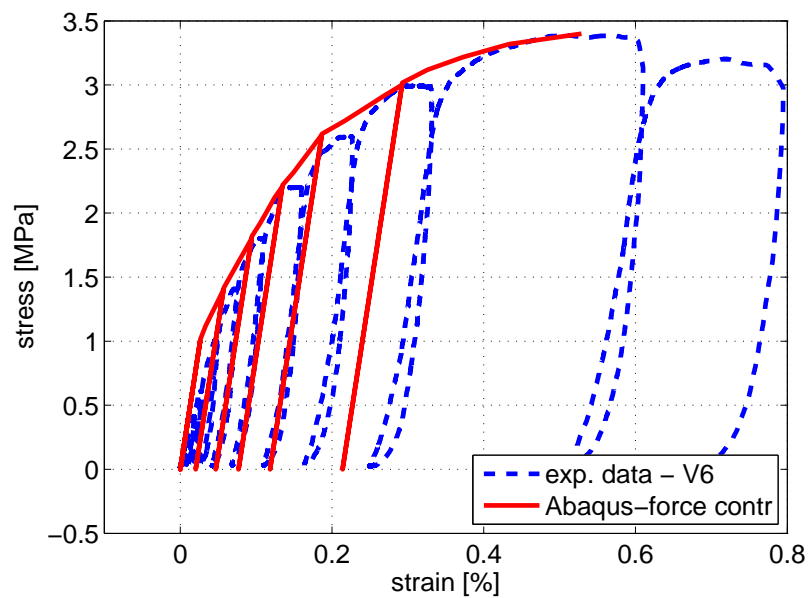Figure 4.14: Behavior of the masonry material model in uni-axial tension

Figure 4.15: Comparison between experimental and numerical data uni-axial cycle

Table 4.4: Load cycles

Time [s]	Pressure [MPa]	Time [s]	Pressure [MPa]
0	0	1560	1.8
20	0.2	1740	0
80	0.2	1800	0
100	0	2020	2.2
160	0	2080	2.2
200	0.4	2300	0
260	0.4	2360	0
300	0	2620	2.6
360	0	2680	2.6
420	0.6	2940	0
480	0.6	3000	0
540	0	3300	3.0
600	0	2360	3.0
700	1.0	3660	0
760	1.0	3720	0
860	0	4060	3.4
920	0	4120	3.4
1060	1.4	4460	0
1120	1.4	4520	0
1260	0	4900	3.8
1320	0	4960	3.8
1500	1.8	5340	0

The results obtained through simulations, especially the ones under cyclic loading, although they are good in the first part of the test, do not lead to satisfactory conclusions.

During diagonal tests, no better results are collected: as can be observed in figure 4.18, the material behaves in the same way as in vertical compression. Infact, no anisotropy can be defined with the concrete damaged plasticity model and this fact leads to the same results obtained in vertical compression tests.
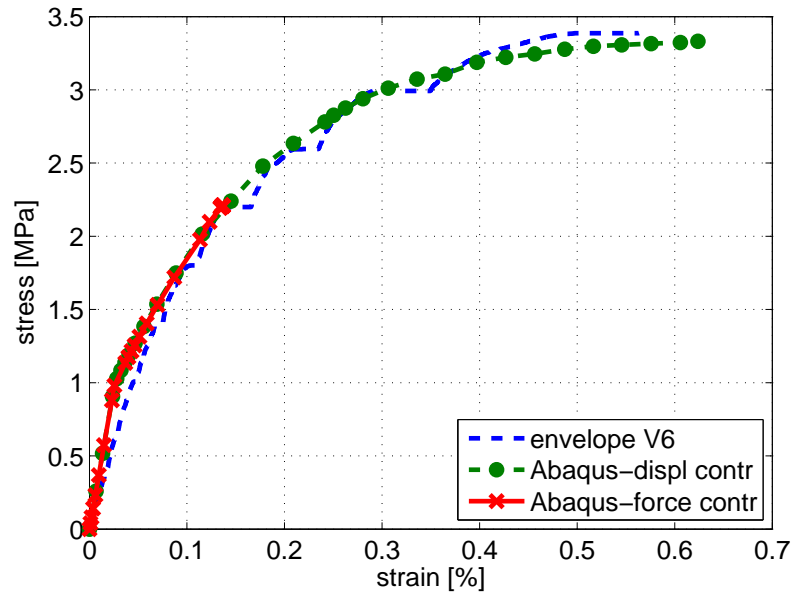
Figure 4.16: Vertical compression of a masonry panel: comparison between experimental and numerical data
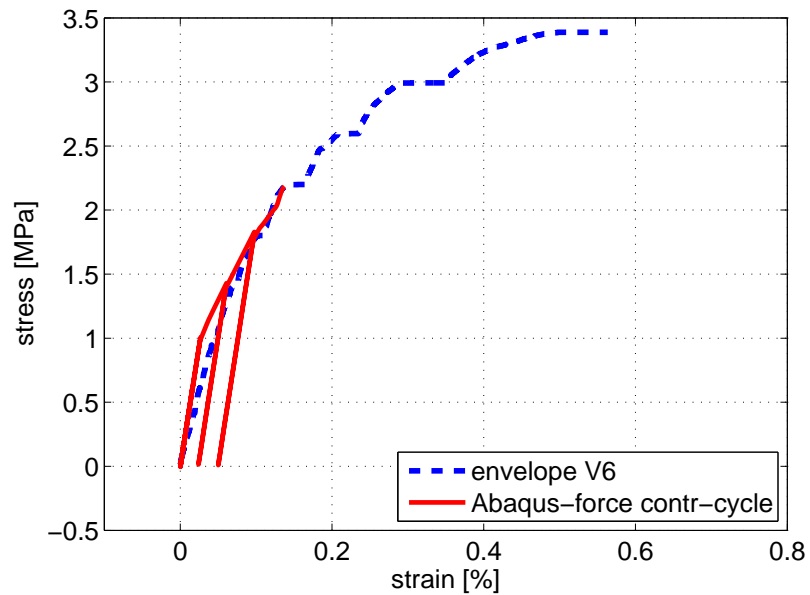

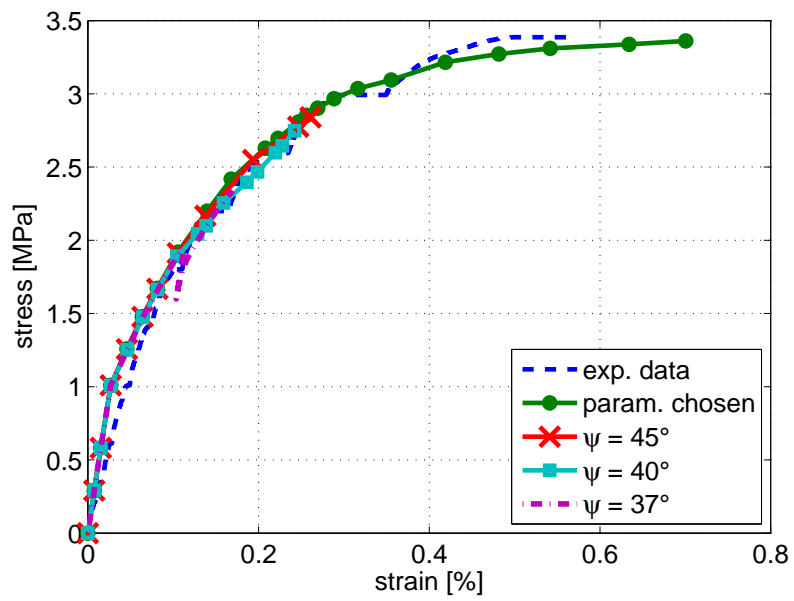Figure 4.17: Comparison between experimental and numerical data uni-axial cycle

Figure 4.18: Comparison between experimental and numerical data: diagonal compression test

4.2.2   Concrete smeared cracking

The concrete smeared cracking model is used to defined the properties of plain concrete outside the elastic range in Abaqus/Standard analysis. This material implementation is good for monotonic loadings under low confining pressure. The most important aspect of the model is cracking and its representation. The data needed to characterize the material behavior are (table 4.5 shows the values used for the simulation):

1. Comp Stress: the absolute value of compressive stress σ_{true};

2. Plastic Strain: the absolute value of plastic strain, which is define as:

$$\varepsilon_{ln}^{pl} = \ln\left(1 + \varepsilon_{nom}\right) - \frac{\sigma_{true}}{E}$$

Table 4.5: Concrete smeared cracking values

Comp Stress $[MPa]$	Plastic Strain
1.05	0
1.50	0.000261
2.13	0.000696
2.60	0.001172
2.94	0.001981
3.25	0.002524
3.31	0.003379
3.39	0.004254
3.38	0.004555
3.34	0.004864
3.31	0.005064

Several sub-options can be selected to better characterize the post-failure behavior for direct straining across the cracks ("Tension Stiffening"), how shear stiffness diminishes as the concrete cracks ("Shear Retention") and, finally, the shape of failure surface ("Failure Ratios").

The "Tension stiffening" option allows to define the strain-softening behavior for cracked concrete, by means of a post-failure stress-strain relation or

by applying a fracture energy cracking criterion. In this case, the post-failure behavior is defined as a function of the displacement at which a linear loss of strength after cracking gives zero stress. This approach is chosen to avoid mesh sensitivity problems related to the stress-strain definition. A value of $u_0 = 5 \cdot 10^{-5}\,\mathrm{m}$ is introduced.

When crack occurs, the material's shear stiffness diminishes. This effect can be defined specifying the reduction in the shear modulus as a function of the opening strain across the crack. A reduced shear modulus for closed cracks can also be defined. When "Shear Retention" is not defined, Abaqus/Standard automatically assumes a full shear retention material, which is true in case where the response does not dependent on shear retention. The data required are:

1. "Rho_close": ρ^{close} is the multiplying factor that defines the modulus for shearing of closed cracks as a fraction of the elastic shear modulus of the uncracked concrete (default $\rho^{close} = 1$)

2. "Eps_max": ε^{max} is the maximum direct strain across the crack (default: full shear retention).

For the first simulation, the default values are used.

The "Failure Ratios" are used to define the shape of the failure surface:

1. "Ratio 1" is the ratio of the ultimate bi-axial compressive stress to the uni-axial compressive ultimate stress (default 1.16)

2. "Ratio 2" is the absolute value of the ratio of uni-axial tensile stress at failure to the uni-axial compressive stress at failure (default 0.09)

3. "Ratio 3" is the ratio of the magnitude of a principal component of plastic strain at ultimate stress in bi-axial compression to the plastic strain at ultimate stress in uni-axial compression (default 1.28)

4. "Ratio 4" is the ratio of the tensile principal stress value at cracking in plane stress, when the other nonzero principal stress component is at the ultimate compressive stress value, to the tensile cracking stress under uni-axial tension (default $1/3$)

Starting from default values, after some compression tests, the parameters shown in table 4.6 were chosen.

Table 4.6: Failure Ratios

Ratio 1	Ratio 2	Ratio 3	Ratio 4
2	0.041	1.28	1.45

Tests shown in figures 4.19 and 4.20 are carried out for a jointed specimen, to see how different parameters value can change the "equivalent masonry" behavior. In all diagrams only one parameter is made to vary while others are kept fixed.
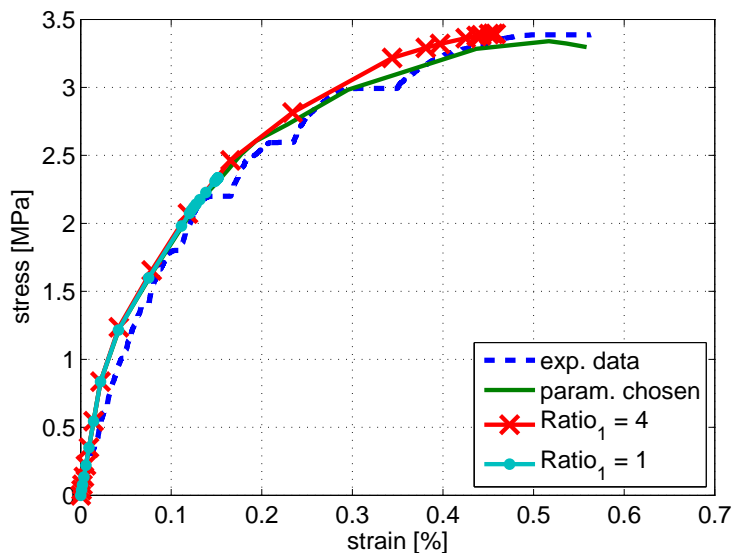

Figure 4.19: Comparison with different value of "Ratio 1" (compression)

The following figures (4.21, 4.22, 4.23, 4.24, 4.25) show the results achieved in force (and displacement) control for uni-axial compression, tensile and cyclic tests and simulations performed on the jointed specimen. As in the previous case, no problems raised neither in the uni-axial case nor during the compression of the specimen trapped to the base. However, with cyclic loading, the simulation stops after a few cycles. Several trial were done with different time increments Δt but results do not change and analysis aborts at the same point. This fact is due to less robustness of the material implementation.
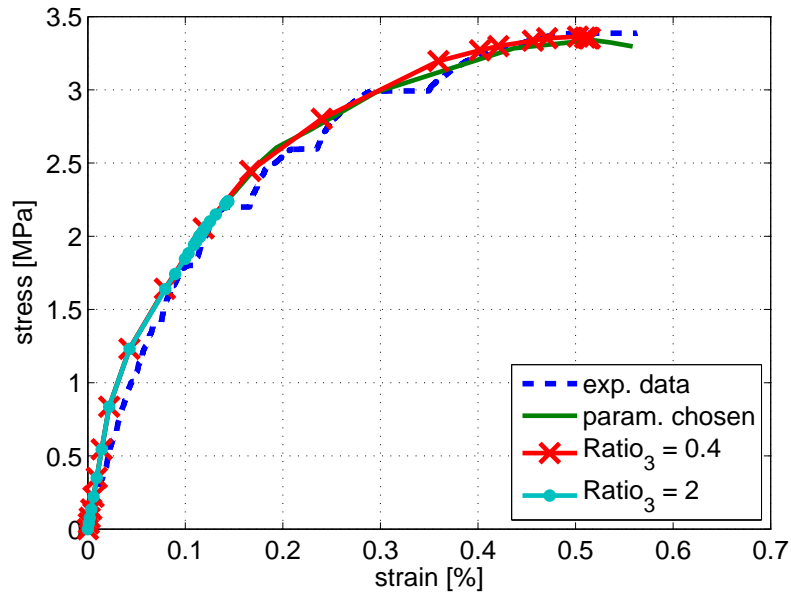
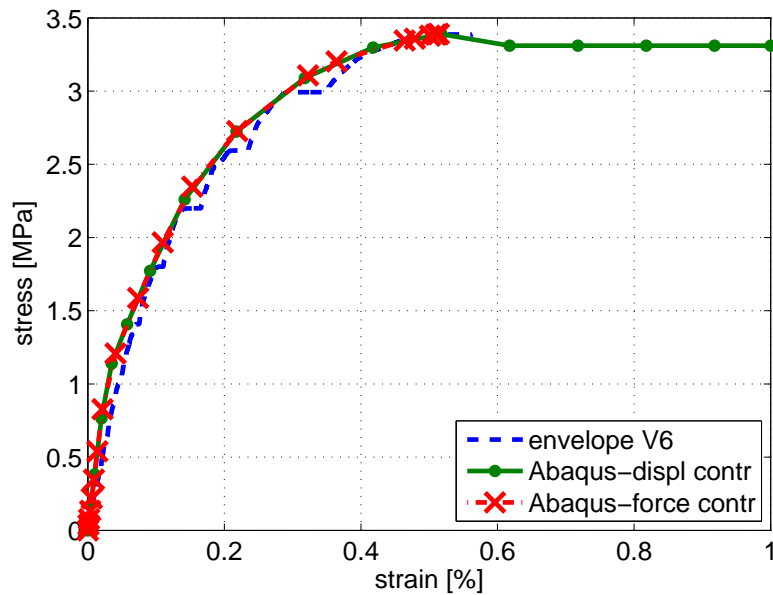Figure 4.20: Comparison with different value of "Ratio 2" (compression)

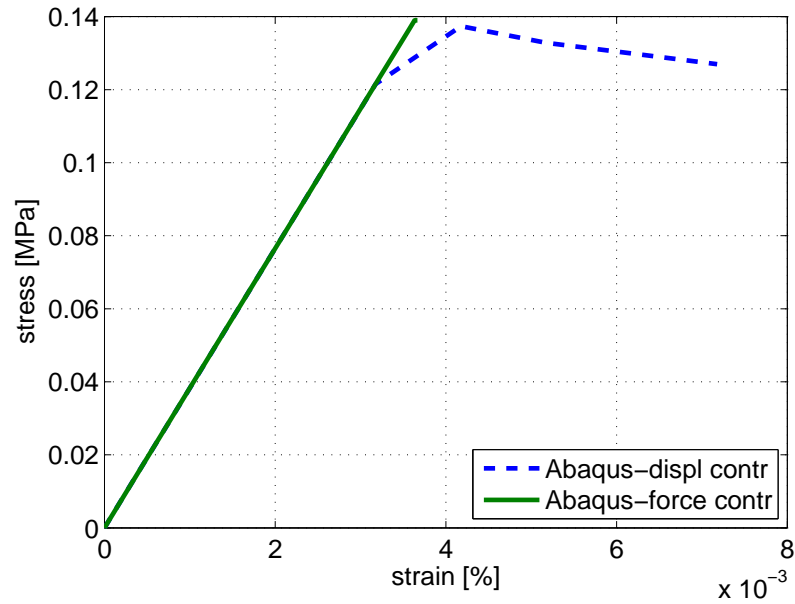Figure 4.21: Comparison between experimental and numerical data in uni-axial compression

Figure 4.22: Behavior of the masonry material model in uni-axial tension
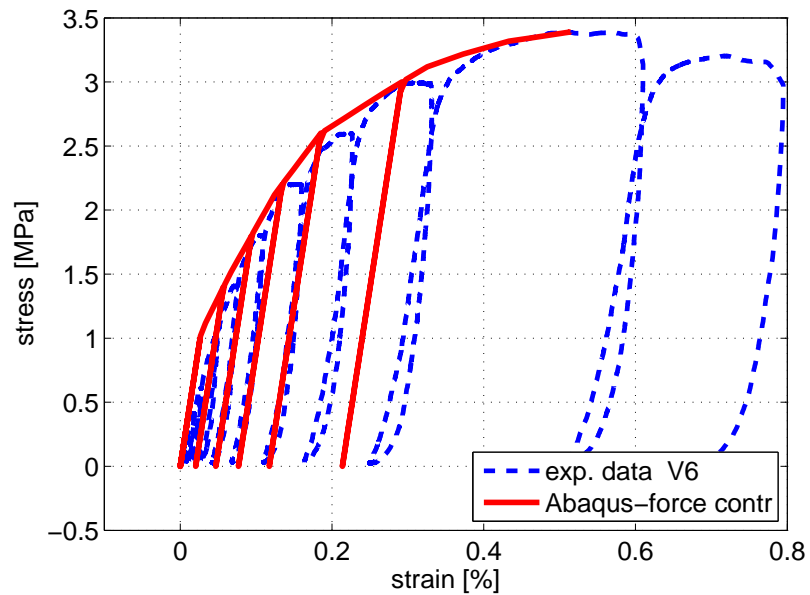

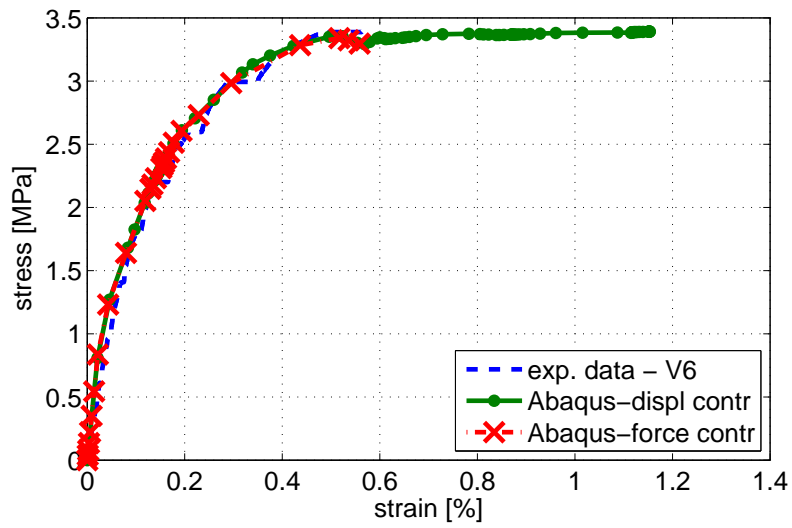Figure 4.23: Comparison between experimental and numerical data in uni-axial cycle

Figure 4.24: Comparison between experimental and numerical data of a wall specimens in compression
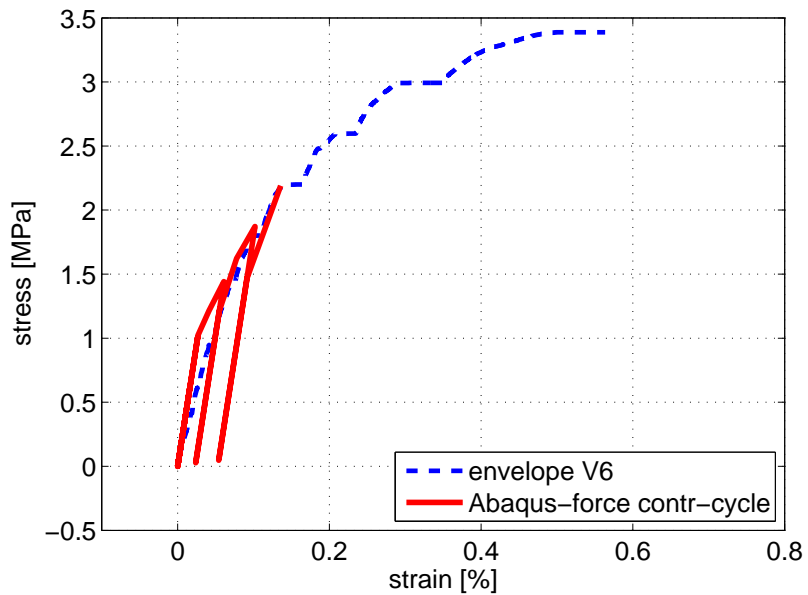

Figure 4.25: Comparison between experimental and numerical data of a wall specimens during loading cycle

Also for the concrete smeared cracking model, during diagonal tests, no better results are collected: the material still behaves in the same way as in vertical compression. Infact, no anisotropy can be defined with the concrete damaged plasticity model and this fact leads to the same results obtained in vertical compression tests.
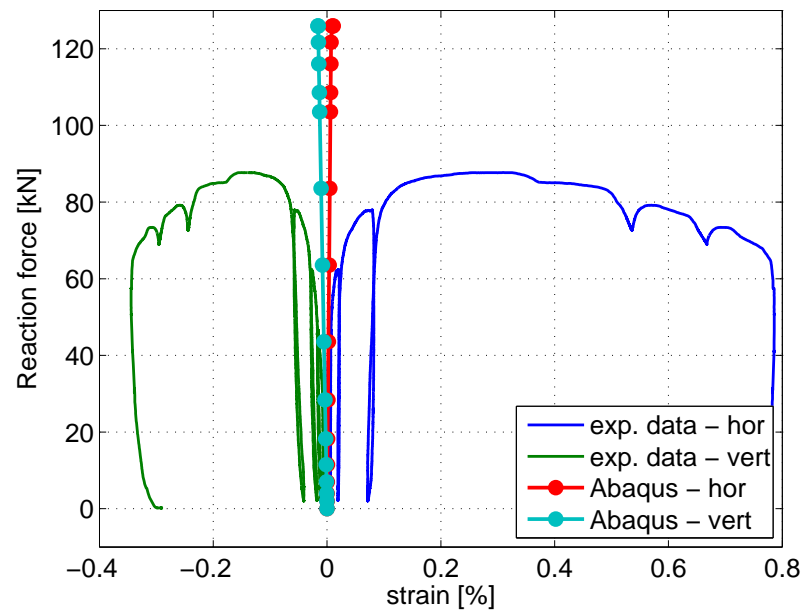

Figure 4.26: Comparison between experimental and numerical data: diagonal compression test

Chapter 5

A User Model take from literature

As can be seen from results described in Chapter 4, materials already implemented in Abaqus do not allow to easily model masonry behavior. Masonry needs a particular constitutive model able to take into account all the characteristics already described, such as the abilities to:

1. describe different behavior in tension and compression;

2. simulate non-linear behavior in plastic branch;

3. simulate anisotropic behavior.

Numerical results in monotonic and cyclic uni-axial tests well simulate the masonry behavior available from experimental tests. Besides that, when boundary conditions change, numerical problems do not allow to simulate the masonry's real behavior.

The literature presents a study carried out by Dhanasekar and Haider[3]. In their paper, an explicit finite element modeling technique able to simulate non-linear events is presented. The object of their research was masonry shear walls first tested and then modeled through the use of Abaqus.

The model includes a user subroutine able to simulate masonry behavior. Abaqus/Explicit provides an interface (VUMAT in Abaqus/Explicit, UMAT in Abaqus/Standard) able to link the user material subroutine with the analysis

program. The material was then implemented as a FORTRAN program and incorporated as a VUMAT subroutine.

However explicit procedures are developed to solve dynamic problems such as impact events where inertia is the most important character in the solution, while tests modeled are pseudo-static. But, besides that, this procedure has also worked out good solutions in static problems if several precautions are taken during analysis.

Static solutions consider the time period, but it is not efficient to perform analysis in natural scale. For this reason, events must be sped up without involving inertia effects. Some option can be used for achieving this purpose, such as increasing the loading rate and the mass density. Moreover for avoiding sudden movements which cause inaccuracy in solutions, loads must be applied as smooth as possible. Abaqus allow user in this work with the option "smooth step amplitude".

Another important check to see if the explicit analysis gives compatible static solutions regards the energy of the system analyzed: it should be that the kinetic energy stays is less than 10% of the Internal energy of the system. To have static solution the density has been increased with a factor of g^2.

The starting point for the VUMAT was Lourenço macro-modeling [10] briefly summarized in section 2.5 and here described in more details.

Lourenço's plane-stress model considers, a compressive yield criterion (derived from Hill yield surface) associated with a localized fractured process, and a tensile yield criterion (that refers to Rankine yield surface) associated to a more distributed fracture process[1].

Hill-type criterion   In compression a Hill-type criterion is used. It must be simple and able to features different compressive strength along x and y directions, thus it is:

$$f_2 = A\sigma_x^2 + B\sigma_x\sigma_y + C\sigma_y^2 + D\tau_{xy}^2 - 1 = 0 \qquad (5.1)$$

---

[1]During these simulations the element used are CPS4R, that means 4-node bi-linear plane stress quadrilateral, reduced integration, hourglass control (for more details see [23])

A, B, C and D are material parameters defined as functions of the yield values $\sigma_{cx}(k_c)$ and $\sigma_{cy}(k_c)$ along the material axes x and y :

$$A = \frac{1}{[\sigma_{cx}(k_c)]^2} \qquad\qquad B = \frac{\beta}{[\sigma_{cx}(k_c)]\,[\sigma_{cy}(k_c)]}$$

$$C = \frac{1}{[\sigma_{cy}(k_c)]^2} \qquad\qquad D = \frac{\gamma}{[\sigma_{cx}(k_c)]\,[\sigma_{cy}(k_c)]}$$

k_c is a scalar able to control hardening and softening, while β is responsible of rotation of the yield surface around the shear stress axis and γ of the shear stress contribution to failure.

Rankine-type criterion   In tension a Rankine-type yield criterion for orthotropic material is used with different tensile strengths along x and y directions:

$$f_1 = \frac{(\sigma_x - \sigma_{tx}(k_t)) + (\sigma_y - \sigma_{ty}(k_t))}{2} + \sqrt{\left(\frac{(\sigma_x - \sigma_{tx}(k_t)) - (\sigma_y - \sigma_{ty}(k_t))}{2}\right)^2 + \alpha\tau_{xy}^2}$$

$$(5.2)$$

where α is a parameter able to control the shear stress contribution to failure and given as a function of the uni-axial tensile strengths f_{tx} and f_{ty} and the pure shear strength τ_u^2:

$$\alpha = \frac{f_{tx} \cdot f_{ty}}{\tau_u^2}$$

$\sigma_{tx}(k_t)$ and $\sigma_{ty}(k_t)$ are the exponential tension softening parameters for the two normal directions given by:

$$\sigma_{tx} = f_{tx} \exp\left(-\frac{h \cdot f_{tx}}{G_{fx}} \cdot k_t\right) \qquad\qquad \sigma_{ty} = f_{ty} \exp\left(-\frac{h \cdot f_{ty}}{G_{fy}} \cdot k_t\right)$$

h is the characteristic length of elements (it depends on the mesh) and G_{fx} and G_{fy} are the fracture energies of masonry along the x and y directions.

Parameters   This anisotropic composite yield criterion needs several parameters to be identified. In particular, seven strength parameters, such as f_{tx}, f_{ty}, f_{cx}, f_{cy}, α, β and γ, and five inelastic parameters, such as G_{fx}, G_{fx}, G_{fx}, G_{fx} and k_p. Figures 5.1 and 5.2 show tests needed to calibrate the model. With these tests, the model parameters α, β and γ are:

$$\alpha = \frac{1}{9} \cdot \left(1 + 4\frac{f_{tx}}{f_\alpha}\right)\left(1 + 4\frac{f_{ty}}{f_\alpha}\right)$$

$$\beta = \left[\frac{1}{f_\beta^2} - \frac{1}{f_{cx}^2} - \frac{1}{f_{cy}^2}\right]f_{cx}f_{cy}$$

$$\gamma = \left[\frac{16}{f_\gamma} - 9\left(\frac{1}{f_{cx}^2} + \frac{\beta}{f_{cx}f_{cy}} + \frac{1}{f_{cxy}^2}\right)\right]f_{cx}f_{cy}$$
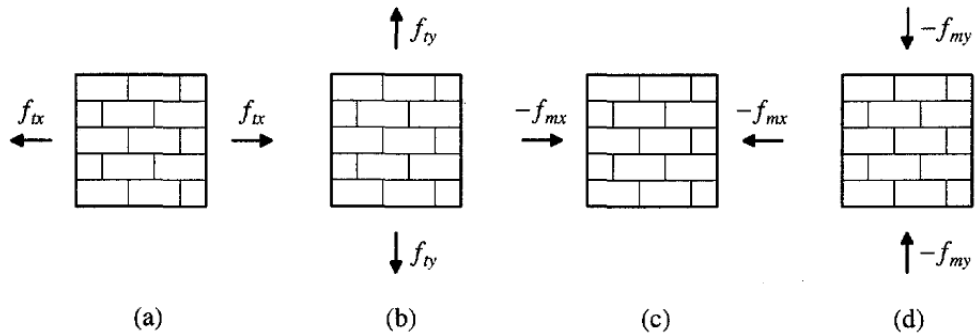

Figure 5.1: Tests to calibrate the model: uni-axial tension (a) parallel to bed joints and (b) normal to bed joints; uni-axial compression (c) parallel to bed joints and (d) normal to bed joints [10]

The VUMAT subroutine described in [3] needs 21 parameters for describing the masonry material model: table 5.1 shows and describes them. Values reported are the ones used by Haider in [15] for the analyses of wide spaced reinforced masonry (referred as WSRM) and unreinforced masonry panels (URM). The masonry considered is made up of clay blocks in single leaf

Energy for compression failure parallel to bed joints G_{fcx} and normal to bed joints G_{fcy} are calculated from the relation proposed by Lourenço [10]:

82

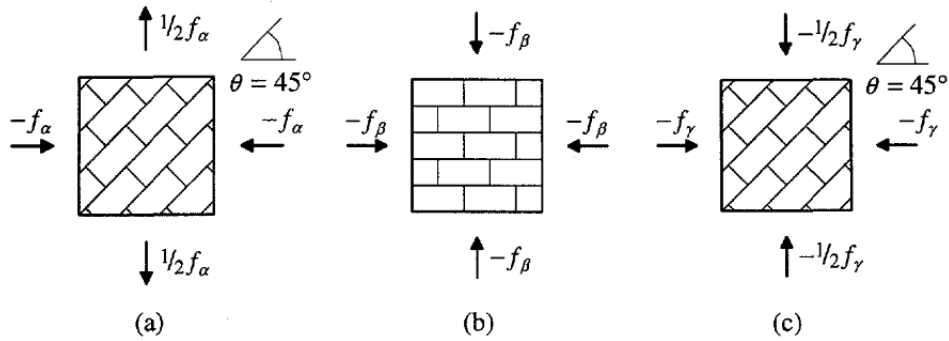Figure 5.2: Possible tests to calibrate the model and calculate (a) parameter α, (b) parameter β and (c) parameter γ, [10]

$$f_{ci} = \left[\frac{75}{67} \frac{G_{fci} E_i}{h} \right]^{0.5}$$

The fracture energies G_{tx} and G_{ty} come from:

$$f_{ti} = \left[\frac{G_{fi} E_i}{h} \right]^{0.5}$$

Finally, the shear modulus is defined as:

$$G = \frac{\sqrt{E_x E_y}}{2 \left(1 + \nu \right)}$$

All these parameters can be easily determined with the tests described before (see figures 5.1 and 5.2), but unfortunately no data referring to this characteristics are available now on our type of masonry which is really different from the one tested in [15, 3]. Moreover, data need for a good calibration of the model cannot be determined from the information already derived from experimental tests.

Besides that, several attempts were done to better know the subroutine and see if results described by Dhanasekar and Haider [15, 3] are reproducible. Infact, many problems arise starting from the Abaqus version used in the first part of this work and regarding the interaction between Abaqus and the FORTRAN compiler

Table 5.1: Material parameters for unreinforced masonry

N.	Par.	Value	Units	Description
1	f_{tx}	0.60	MPa	Tensile strength parallel to bed joints
2	G_{tx}	1.00	$\mathrm{N-mm/mm^2}$	Fracture energy parallel to bed joints
3	f_{ty}	0.35	MPa	Tensile strength normal to bed joints
4	G_{ty}	0.50	$\mathrm{N-mm/mm^2}$	Fracture energy parallel to bed joints
5	α	1.25	-	Shear stress contribution factor to the tension failure
6	α_g	1.00	-	Mathematical variable for plastic flow of masonry
7	f_{cx}	3.00	MPa	Compressive strength parallel to bed joints
8	G_{fcx}	0.302	$\mathrm{N-mm/mm^2}$	Energy for compression failure parallel to bed joints
9	f_{cy}	18.00	MPa	Compressive strength normal to bed joints
10	G_{fcy}	4.35	$\mathrm{N-mm/mm^2}$	Energy for compression failure normal to bed joints
11	β	-1.17	-	Bi-axial compressive strength factor
12	γ	4.00	-	Shear stress contribution factor to compression failure
13	h		mm	Characteristic length of critical elements
14	k_p	0.0025	-	Strain compression failure
15	E_x	6000	MPa	Young's Modulus of masonry parallel to bed joints
16	E_y	15000	MPa	Young's Modulus of masonry normal to bed joints
17	$E_z{}^2$	1E-03	MPa	Young's Modulus of masonry along thickness direction
18	ν_x	0.20	-	Poisson's Ratio of masonry parallel to bed joints
19	ν_y	0.20	-	Poisson's Ratio of masonry normal to bed joints
20	$\nu_z{}^3$	1E-07	-	Poisson's Ratio of masonry along thickness direction
21	G	3953	MPa	Shear Modulus of masonry

needed to run the analysis.

The first comparison made regards the modal analysis done to compute the natural frequency of the URM; figure 5.3 shows the first mode of vibration from [15] (natural frequency equal to $101.78\,\mathrm{Hz}$, natural time period equal to $0.01\,\mathrm{sec}$) and figure 5.4 shows results obtained during simulations (natural frequency equal to $102.78\,\mathrm{Hz}$, natural time period equal to $0.01\,\mathrm{sec}$)

Another test was made for evaluate if strain and stress patterns are the comparable. After $2\,\mathrm{mm}$ of horizontal displacement, results are shown in figures 5.6 and 5.7, while figure 5.5 shows patters from Haider's simulations. The patterns are quite different and these differences may be due to different characteristic lengths and different step time used in the analyses. Also figure 5.8 and figure 5.9 represent the normalized horizontal load versus the horizontal displacement and

show that results are different and the cause is that a more accurate study should be made on step time and on the right characteristic lengths. The normalized load is:

$$H = \frac{H_{Fem}}{0.22 \cdot \sqrt{f_m} \cdot A_g} \cdot 10^3$$

where H_{Fem} is the horizontal load calculated from the model, f_m is the peak value of compressive strength equal to $13.7\,\text{MPa}$ and $A_g = t_w \cdot L$ is the gross area of the wall.

Anyway it must be said that after this preliminary analysis, this VUMAT subroutine is able to see masonry behavior during in-plane shear tests, but a more accurate study on step time needed and on characteristic lengths should be made. This subroutine is a powerful tool and might lead to good results, but it can be used only for evaluating in-plane behavior and it is not able to simulate out-of-plane masonry behavior.
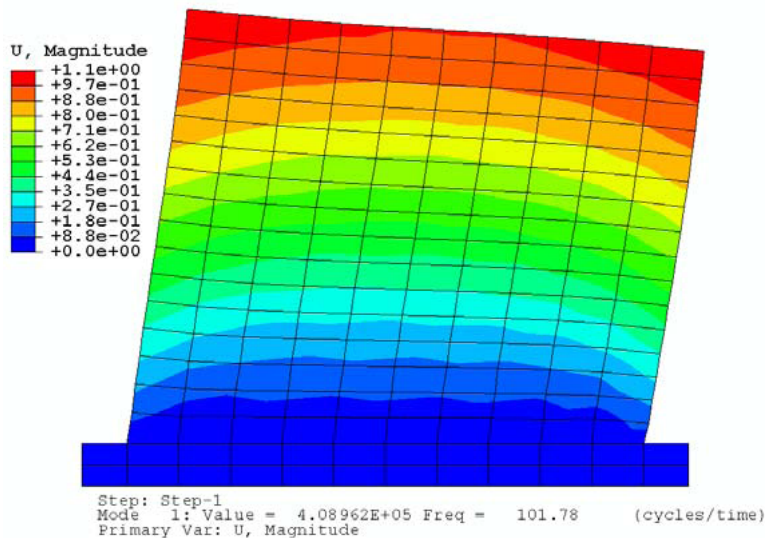
Figure 5.3: First mode of vibration of URM from [15]
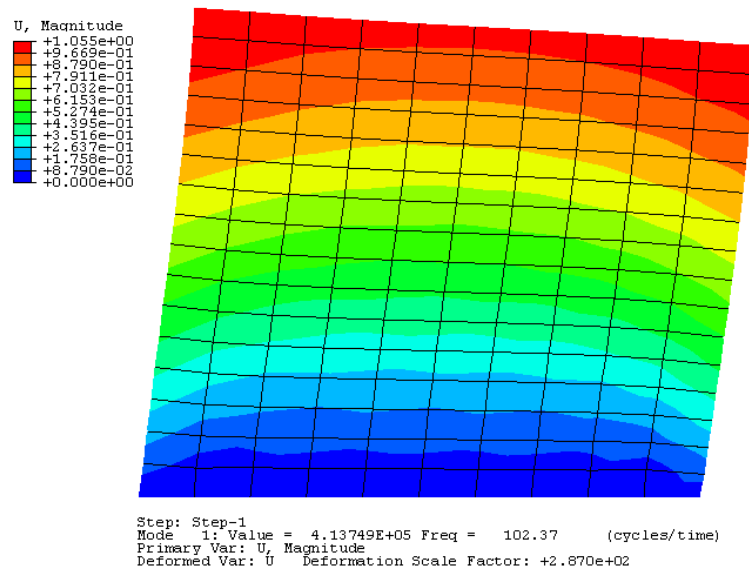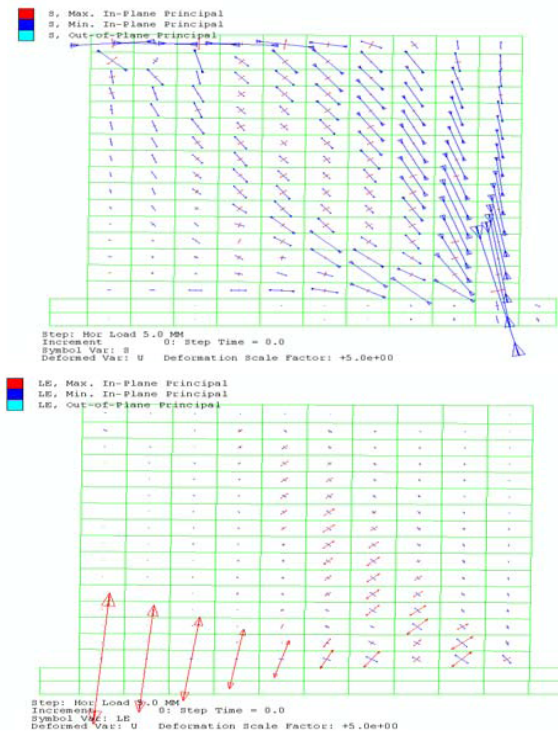
Figure 5.4: First mode of vibration of URM

Figure 5.5: Stress (upper side) and strain (lower side) pattern after $5\,\text{mm}$ of horizontal displacement [15]
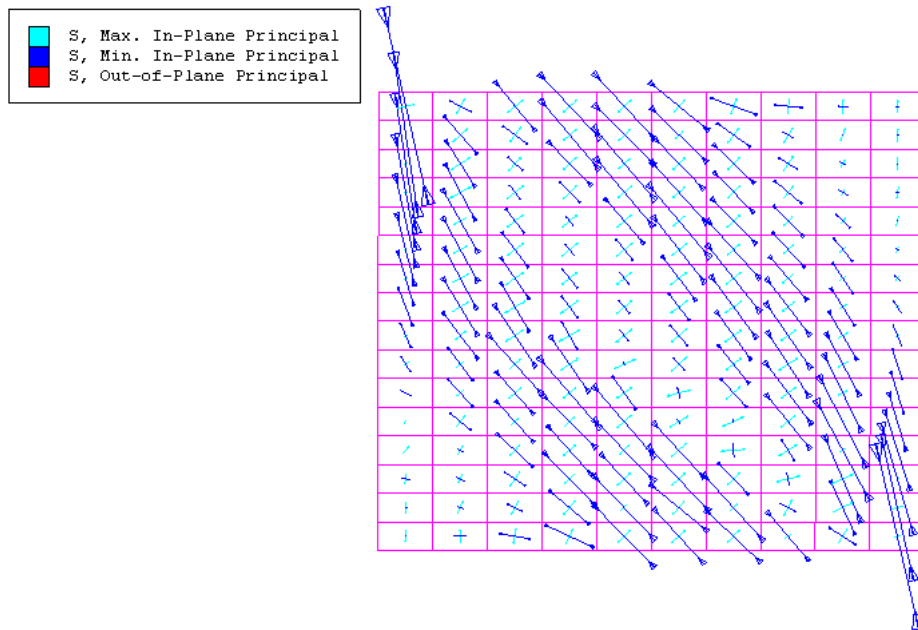
Figure 5.6: Stress pattern after $2\,\mathrm{mm}$ of horizontal displacement
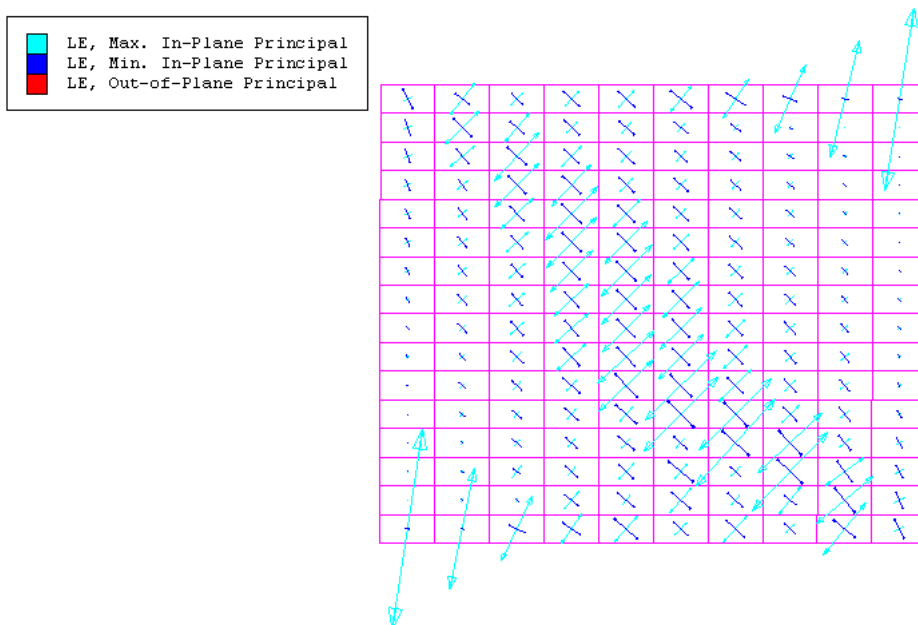
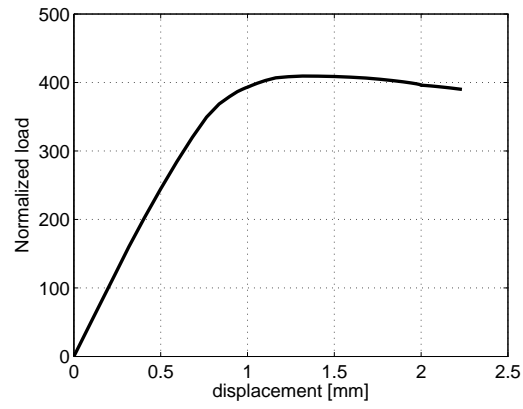Figure 5.7: Strain pattern after $2\,\mathrm{mm}$ of horizontal displacement

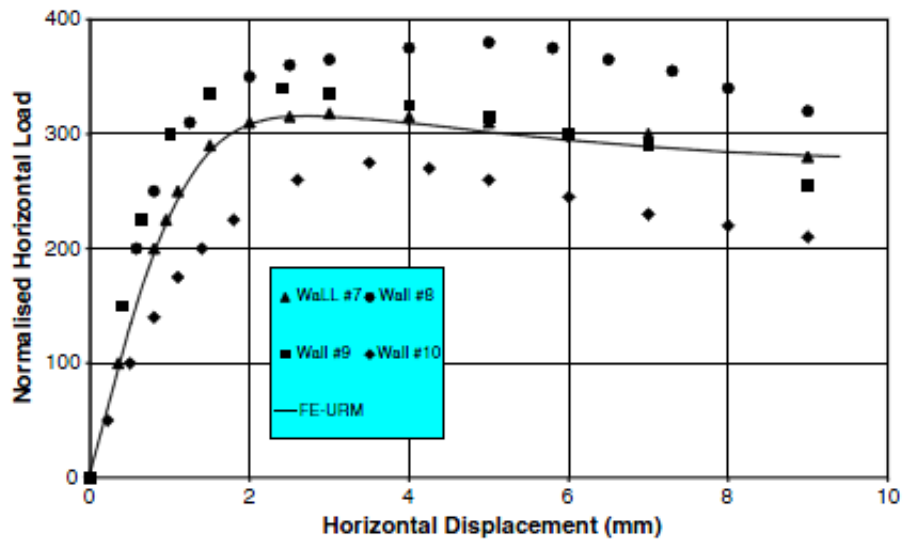Figure 5.8: Normalized load versus horizontal displacement

Figure 5.9: Normalized load versus horizontal displacement [3]

Chapter 6

Conclusions

In Chapter 2 a classification of methods available in literature is carried out. Here, two new method are briefly described. The first one (section 6.1) is a new method that comes from the analyses of masonry modeling problems and is intended to overcome them. The second method (section 6.2) is now used to model rocks, but it might be good also for masonry.

6.1 Localized damaged model

Finite element analysis of masonry usually do not provide a realistic simulation of damage and usually mesh dependence can cause many problems. To overcome these aspects Pelà, Cervera and Roca [21] propose a smeared model able to capture individual discrete cracks. Through a cracking tracking algorithm the crack is forced to develop along a single row of finite elements.

The localized damaged model takes also into account the orthotropic behavior of masonry with a new and original method which map stress and strain tensors from the anisotropic real space to a scaled isotropic space. In this way there an important gain from a computational point of view: the problem is solved in the scale spaced and then mapped back to the anisotropic space.

The plane stress macro-model proposed in [21] is able to simulate several important characteristic of the masonry material, such as:

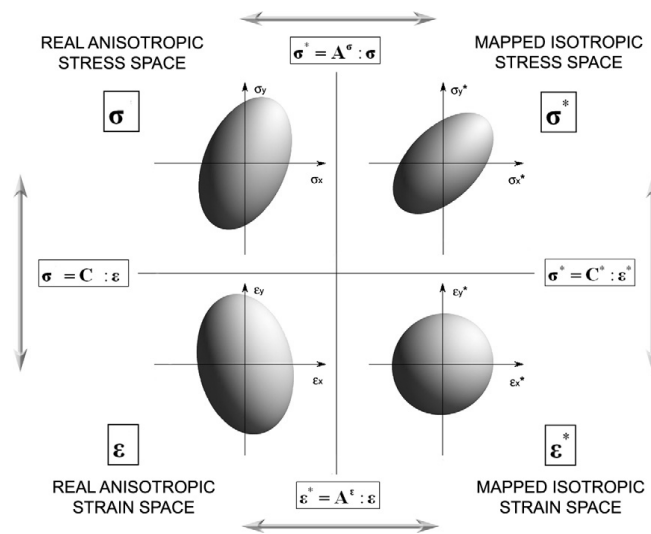1. the undamaged material is seen as an elastic orthotropic material;

Figure 6.1: Relationship between the real anisotropic space and the mapped isotropic space [21]

2. there are two main natural direction, parallel and normal to bed joints, along which the material model has different strength and different softening behavior; the model uses in the mapped space, the Rankine criterion in tension and the Faria criterion in compression;

3. the damaged stiffness affects the unloading and the reloading processes;

4. during loading cycles with alternate load, the stiffness recovers when cracks close.

The model has been formulated for the two-dimensional case but it can be extended to the three-dimensional case, if additional material parameters are added.

6.2 Micro-modeling

Research on masonry behavior during earthquake is still an open field: other numerical method can be used in modeling and more aspect can be studied.

One of the most important aspect which is not included in this thesis regards masonry's fracture. This topic is very important and need special numerical method aim at modeling failure, fracture and fragmentation.

90

The combined finite-discrete element method (FEM-DEM) is an innovative technique that allow modeling of failure and collapse of structural system.

The FEM-DEM method combines aspects taken from both finite elements and discrete elements. In this innovative hybrid technique, each discrete element is discretized into finite elements, that means that there is a finite element mesh associated with each discrete element. Moreover, the finite elements allow to model the continuum behavior, while through discrete elements, the discontinuum behavior is analyzed.
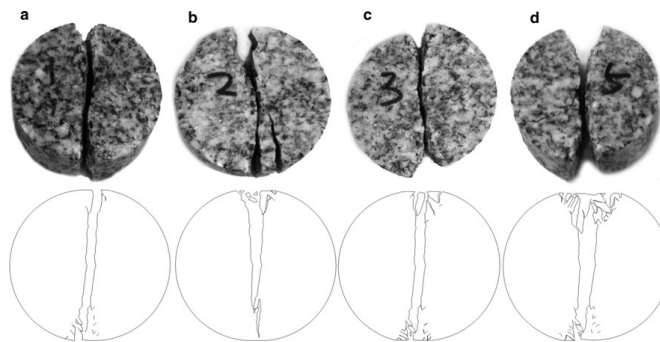

Figure 6.2: Fracture pattern of the samples failed in experiments (*top*) and simulated (*bottom*)

The contact between the interacting domains is defined as in the discrete element method, but the contact domains are discretized with finite elements as the solid domains and discretized contact solutions are used for contact detection and contact interaction. The contact detection consist of a set of procedures and algorithms aimed at eliminating domains that are at such distances apart that there could not be contact between them, listing all domains that are close to each other and can be in contact. For this reason, the method has a great computational effort.

The FEM/DEM procedure can be summarized as follow:

- the FEM discretization must capture pre-failure behavior;

- after failure and collapse, the same FEM discretization must capture interaction between failing and collapsing structural elements.

This new technique has already been used for structural failure [17] and for modeling of rock dynamics problems [14]. Figure 6.2 compares experimental

results and FEM/DEM simulations of Dynamic Brazilian Test on Barre Granite, while figures 6.3 and 6.4 show the experiment carried out to validate the model in [17]. For both cases, results are encouraging; this leads to think that the method could be applied to the masonry, which is a structural material, which behaves more like granular material than concrete. Currently, the major limiting factor for FEM/DEM is the computational power required, but it is intended to develop a version able to overcome this problem.

More detailed descriptions of the methods and experiments done are available in [17] and [14]
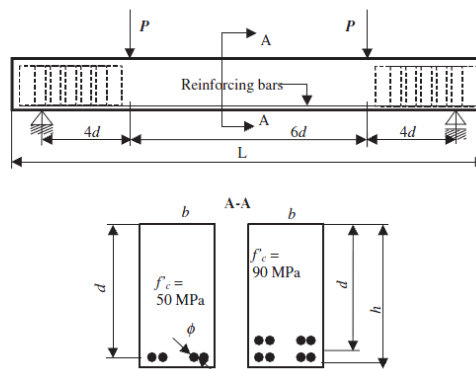

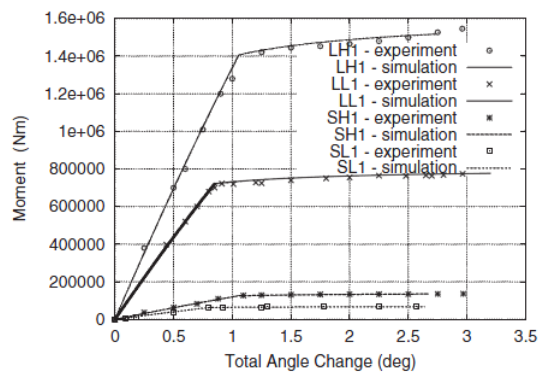Figure 6.3: Loading arrangements, cross section and reinforcing bats for experimental beams in [17]

Figure 6.4: Comparison between experimental and simulation results [17]

Bibliography

[1] Brencich A. & Lagomarsino S., 1998, A MACRO-ELEMENT DYNAMIC MODEL FOR MASONRY SHEAR WALLS. in Pande G et al (eds.) Computer methods in structural Masonry 4. London: E&FN Spon.1998: 67-75

[2] Calderoni, B., Marone, P., Pagano, M., 1987, MODELLI PER LA VERIFICA STATICA DEGLI EDIFICI IN MURATURA IN ZONA SISMICA. Ingegneria sismica, n. 3, pp.19-27.

[3] Dhanasekar, M., Haider, W., 2008, EXPLICIT FINITE ELEMENT ANALYSIS OF LIGHTLY REINFORCED MASONRY SHEAR WALLS. Computers and Structures 86 (15-26)

[4] Dolce M., 1989, SCHEMATIZZAZIONE E MODELLAZIONE PER AZIONI NEL PIANO DELLE PARETI. Corso sul consolidamento degli edifici in muratura in zona sismica, Ordine degli Ingegneri, Potenza.

[5] Gambarotta L. & Lagomarsino S., 1996, DAMAGE MODELS FOR THE SEISMIC RESPONSE OF BRICK MASONRY SHEAR WALLS. PART I: THE MORTAR JOINT MODEL AND ITS APPLICATIONS. Earthq. Engin. and Struct. Dyn., Vol. 26, pp.441-462.

[6] Gambarotta L. & Lagomarsino S., 1997, DAMAGE MODELS FOR THE SEISMIC RESPONSE OF BRICK MASONRY SHEAR WALLS. PART II: THE CONTINUUM MODELS AND ITS APPLICATIONS. Earthq. Engin. and Struct. Dyn., Vol. 26, pp.441-462.

[7] Gambarotta L. & Lagomarsino S., 1997, ON DYNAMIC RESPONSE OF MASONRY PANELS. in Gambarotta L. (ed) Proc. of the National Confer-

enche "La meccanica delle murature tra teoria e progetto", Messina, (in italian)

[8] Giuffré A. (ed.), 1993, SICUREZZA E CONSERVAZIONE DEI CENTRI STORICI IN ZONA SISMICA. Il caso di Ortigia, Laterza, Bari.

[9] Lee, J. and Fenves, G. L., 1998, PLASTIC-DAMAGE MODEL FOR CYCLIC LOADING OF CONCRETE STRUCTURES. Journal of Engineering Mechanics, vol. 124, no.8, pp. 892–900.

[10] Lourenço, P. B., 1996, COMPUTATIONAL STRATEGIES FOR MASONRY STRUCTURES. PhD thesis, Delft University, Netherlands.

[11] Rots, J.G., Lourenco, P., Blaauwendraad, J., 1998. CONTINUUM MODEL FOR MASONRY: PARAMETER ESTIMATION AND VALIDATION. Journal of Structural Engineering 124 (6), 642–652.

[12] Lubliner, J., J. Oliver, S. Oller, and E. Oñate, 1989, A PLASTIC-DAMAGE MODEL FOR CONCRETE. International Journal of Solids and Structures, vol. 25, no.3, pp. 229–326.

[13] Magenes G., Bolognini D. & Braggio C. (a cura di), 2000, METODI SEMPLIFICATI PER L'ANALISI SIMISCA NON LINEARE DI EDIFICI IN MURATURA. CNR-Gruppo Nazionale per la difesa dai Terremoti - Roma

[14] Mahabady, O. K., Cottrell, B. E. and Grasselli, G., 2010, AN EXAMPLE OF REALISTIC MODELLING OF ROCK DYNAMICS PROBLEMS: FEM/DEM SIMULATION OF DYNAMIC BRAZILIAN TEST ON BARRE GRANITE. Rock Mechanics and Rock Engineering.

[15] Haider, W, 2007, In-plane response of wide spaced reinforced masonry shear walls, Ph.D. thesis, Central Queensland University, Australia.

[16] Heyman, J., 1969, THE SAFETY OF MASONRY ARCHES. International Journal of Mechanical Sciences, Volume 11, Issue 4, Pages 363-385.

[17] Munjiza, A., Bangash, T., John, N.W.M., 2004, THE COMBINED FINITE-DISCRETE ELEMENT METHOD FOR STRUCTURAL FAILURE AND COLLAPSE. Engineering Fracture Mechanics, 71(4-6), 469-483.

[18] Magenes, G., Penna, A., Graziotti, F. ,2011a, QUASI-STATIC CYCLIC TESTING OF FULL-SCALE STONE MASONRY SPANDRELS. Report, IUSS Press, Pavia (in print).

[19] Magenes, G., Penna A., Galasco, A., Rota, M., 2011b, DOUBLE-LEAF STONE MASONRY. CHARACTERISATION OF MECHANICAL PROPERTIES AND CYCLIC TESTING OF MASONRY WALLS. Report, IUSS Press, Pavia (in print).

[20] Nuove Norme Tecniche per le Costruzioni, DM 14.I.2008 (in Italian)

[21] Pelà, L., Cervera, M., Roca,P. 2011, CONTINUUM DAMAGE MODEL FOR ORTHOTROPIC MATERIALS: APPLICATION TO MASONRY. Computer Methods in Applied Mechanics and Engineering, Volume 200, Issues 9-12, Pages 917-930.

[22] Penna A., 2002, A MACRO-ELEMENT PROCEDURE FOR THE NON-LINEAR DYNAMIC ANALYSIS OF MASONRY BUILDINGS. Ph.D. Dissertation (in italian), Politecnico di Milano, Italy.

[23] Simulia, ABAQUS ANALYSIS USER'S MANUAL. Providence RI, 2008.

[24] Simulia, ABAQUS/CAE USER'S MANUAL. Providence RI, 2008.

[25] Simulia, ABAQUS EXAMPLE PROBLEMS MANUAL. Providence RI, 2008.

[26] Simulia, ABAQUS KEYWORDS REFERENCE MANUAL. Providence RI, 2008.

[27] Simulia, ABAQUS THEORY MANUAL. Providence RI, 2008.

[28] Tomaževic, M., 1978, THE COMPUTER PROGRAM POR. Report ZRMK, (in Slovene).

[29] Tunseck, V. & Sheppard, P.F., 1980, THE SHEAR AND FLEXURAL RESISTANCE OF MASONRY WALLS. Proceedings of the Research Conference on Earthquake Eng., Skopje.